Chapter 1

Analysis of Cell Divisions Patterns in the Arabidopsis Shoot Apical Meristem

1.1 Introduction

The Arabidopsis SAM is a structure at the tip of the shoot that is responsible for generating almost all of the above-ground tissue of the plant[1]. Its epidermal and subepidermal cells are organized into layers with very few cells moving between layers[2, 3]. When these cells expand they do so laterally, pushing other cells towards the periphery of the meristem. Division in these cells is anticlinal such that each layer remains one cell thick. Since plant cells are bound to each other by common walls and can't move past each other, the position of the walls created during cytokinesis is critical to patterning and morphogenesis at the tissue and organ level.

1.1.1 Qualitative Observations

While the underlying mechanisms that control positioning of the cell plate are not completely known (discussed in detail later), the qualitative properties of meristematic cell division are well documented. Perhaps the three most well known of these observations are those of the 19th century

botanists Wilhelm Hofmeister, Léo Errera, and Julius von Sachs.

1. Errera observed that soap bubbles and plant cells often divide in much the same way; the plane of division corresponds to the shortest path that will halve the volume of the mother cell[4]. According to Errera (1888, section IV) the new wall will be a surface "mit constanter mittlerer Krümmung (= Minimalfläche) [with constant average curvature (minimal area)]". Since then, other authors have also compared plant tissue to soap foam, often suggesting that since the outcome is qualitatively similar, plant cells and soap bubbles may share a common underlying mechanism[5, 6, 7, 8]. In foams, surface tension causes the volume to be maximized while being bound by the least amount of material. Whether plant cells also use mechanical forces to govern locations of new walls has yet to be determined 125 years after Errera's initial observation. Nevertheless, Errera's rule is still used to describe plant cell division patterns. But since this rule does not specify a single, unique location for the new cell wall, more recent authors have added to this that the mother cell divides evenly[9, 10]. With these modifications, Errera's rule is easily quantifiable.

2. Hofmeister observed that new cell walls usually form in a plane normal to the principal axis of cell elongation[11]. This rule is more difficult to quantify because the principal axis of cell elongation is often confused with the direction of growth. Cells are asymmetrical and hence a principal direction of cell elongation can easily be calculated (e.g., the principal axis of inertia or principal component of a segmentation). The assumption is often made that because the cell is more elongated in one direction that the primary growth of the cell has been along that direction, but this is not necessarily the case, as the elongation may be derived from a prior cell division. For example, if a symmetrical square divides into two rectangular cells, this does not mean that the two daughter cells have grown primarily along their longer axis. Quantification of cell growth direction is much more difficult: it requires the observation of matching points over time and varies with the internal and external tensile forces on the cell. It is not clear whether or not the instantaneous direction of cell growth or the longer-term average (e.g., as measured over a significant fraction of a cell generation) is more directly relevant to forming the division plane. Under compression, single cells tend to divide in a plane perpendicular to the long axis of the cell[12] which, similar to Errera's rule, could indicate a mechanical basis for cell wall placement.

3. Sachs observed that new cell walls form in a plane perpendicular to existing cell walls and that the daughter cells are of equal volume[13]. These rules are an accurate description of cells that

have already divided but do not necessarily allow one to predict the plane of division in a cell that has yet to divide since there are often multiple wall positions that fulfil Sachs' rules as illustrated by Minc and Piel[14] in Figure 1.

Other qualitative observations are that cell walls tend to avoid four-way junctions[15] and that cell division planes tend to be staggered, like bricks in a wall[16]. Since chemical signals can be induced by physical interactions such as mechanical stress and strain it is conceivable that these geometric indicators are merely emergent properties of the underlying physico-chemical interaction processes that drives cell division. While most of the geometric observations tend to be true most of the time, none of them are true all of the time, and it is not possible for all of them to be true at once. For example, the actual growth direction is rarely in alignment with the principal geometric axis of the cell and hence the division cannot simultaneously satisfy shortest length and perpendicularity requirements. Such conflicting results can in principle be resolved by minimizing a sum of potential functions[17], and insight into the underlying mechanisms can often be gained by examining the results of the optimization.

1.1.2 Mechanism of Cell Plate Positioning

The earliest work to determine the mechanism of division plane formation in plant cells were observations of (what would be later known as) the mitotic spindle and phragmoplast (the scaffold for the cell plate that eventually becomes the wall)[18, 19, 20]. These early observations lead to the discovery of the preprophase band, which is the earliest known indication of the future location of the phragmoplast[21]. The preprophase band is a gathering of microtubules into a circular (not spherical) structure at the periphery of the cell, just inside the plasma membrane. The accumulation of micorubules forms bundle structures[22, 23] that probably also include γ-tubulin ring complex elements as well as other microtubule binding proteins[24, 25, 26].

Though there is still not much evidence that the preprophase band is directly responsible for positioning the phragmoplast, it has been shown to be necessary for non-random positioning in most Arabidopsis cell types aside from endosperm[27] and meiocites[28]. In tissue culture Arabidopsis cells often lack a preprophase band and exhibit random phragmoplast positioning [29]. Additionally, tissue treated with small molecules that depolymerize microtubules and tissue with genetically inhibited microtubules also exhibit random phragmoplast positioning [30, 31, 32, 33, 34].

So the cell plate, in most cases, is positioned by the organization of the preprophase band. But this

changes the question "how is the cell plate positioned?" to "how is the preprophase band positioned?" This is accomplished through a variety of proteins homologous to those in animal centrosome complexes even though plant cells lack centrosomes. For example, the TON1 proteins interact with the preprophase band, the cortical microtubules and the CEN proteins[35]. TON2 mutants display disorganization of the interphase cortical microtubule array and also lack a preprophase band[36]. MOR1, a microtubule binding protein of the MAP25 class, is also required for orderly cortical microtubule arrays and mutants display random phragmoplast orientation[37]. CLASP is typically found along microtubules enriched at the positive end of microtubules[38] and near the plasma membrane and prevents edge-induced microtubule depolymerization, a process that occurs when a microtubule oriented perpendicular to the plasma membrane encounters a sharp cell edge such as those found at a three way junction[39]. Other plant-specific proteins (non-homologous to animal proteins) are involved as well, such as many members of the TRM family which link the TON1 proteins to microtubules[40].

These proteins are all necessary parts of a system guiding the cytoskeleton of Arabidopsis cells but still don't provide a mechanism by which positioning of the preprophase band and phragmoplast are controlled. For a short time CLASP looked like a possible master regulator of preprophase band positioning. It was thought to localize laterally within growing cells and be necessary for the maintenance of the cortical microtubules in such a way that promotes anticlinal (parallel to the apical basal axis) divisions, at least within the meristem. Further, it was suggested that MAP65 expression causes CLASP to relocate within the cell and subsequently causes *periclinal* (perpendicular to the apical basal axis) divisions[41]. This provided a direct link between the transcription of a gene and the positioning of the division plate and provided an obvious mechanism for different cell types to alter their division patterns. But this paper as well as another related paper[42] were retracted because the data were faked so I find it unlikely that this particular connection is true.

While we still don't have a molecular mechanism for the positioning of the cell plate, it is evident that microtubules play a major part in the process. And since there is strong evidence that mechanical forces experienced by cells can influence the position of the cytoskeleton, it is tantalizing to think stress or strain act as regulators of the cell plate positioning process.

1.1.3 Stress and Strain as Controlling Factors in Cell Division

If mechanical forces are the significant driver of wall placement this would suggest that (a) the plant cells can somehow detect and respond to mechanical stress/strain, perhaps through some intermediary signalling mechanism, and that (b) the geometric observations are indicators that emerge as a consequence of the physically induced signalling and not the ultimate cause of cell division. None of these observations are sufficient to predict the orientation of the division plane with any confidence; in fact, they are sometimes in conflict, e.g., the current growth direction at any given time results from a complex interaction of mechanical stresses and strains and is not necessarily in alignment with the principal geometric axis of the cell and hence the division cannot simultaneously satisfy shortest length and perpendicularity requirements. Conflicting results can in principle be resolved by minimizing a sum of potential functions[17].

1.1.4 Modeling

Additionally, recent work by Besson and Dumais suggests that cell division in plants is inherently random[9]. The new wall tends to find a global minimum length but in situations where there are multiple similar local minima the global minimum is not necessarily chosen.

Previously we looked at cell divisions in the shoot meristem using two dimensional maximum intensity projections[43]. Some of the results from that work may have been biased due to the inconsistent perspective on cells in the peripheral zone compared to the center created by projecting a 3D object into 2D space. Since the meristem is dome-shaped, when projecting the meristem from the top the cells in the center are viewed perpendicularly while the cells towards the edges are viewed at an angle. This non-perpendicular viewing angle distorts the lengths of the cell walls and the angles at which the walls join each other. To rectify that problem the geometry of the cells must be examined in 3D. Here we expand on earlier work with new image processing techniques to analyze the division patterns in 3 dimensions. By using the image processing software MorphoGraphX[44] we were able to reconstruct the cell boundaries in the first layer of a growing SAM [44].

Having a 3-dimensional model of the structure of the L1 layer over time allowed us to generate a model composed of a set of functions, each incorporating a different feature from the observed cell divisions. The functions each contribute a single term to a greater potential function and new walls are predicted to form where the combined potential is reduced. This model also brought to light some of the shortcomings of previously proposed plant cell division rules. Additionaly, these data

allowed us to make new observations of the dynamics of cell expansion and division in different regions of the SAM.

1.2 Methods

1.2.1 Plants

Seeds from the pUBQ::tdTomato-29-1 line in the L-er background were sterilized with 70% ethanol and added to agar plates containing MS and sucrose (30g/L). After a 3-day vernalization at 4°C, seeds were germinated under constant light at room temperature. 10 days after germination, plants were transferred to boxes containing solid growth medium and grown under constant light at room temperature. Plastic boxes 4cm high were prepared under sterile conditions and filled 1cm high with a growth media consisting of MS, MS vitamins, and agar. 1 thin layer of agar without MS was poured on top of the solid MS agar.

1.2.2 Time-Series Images

Laser scanning confocal images of four different Arabidopsis meristems were taken at 2 hour intervals during which 207 cell divisions were observed. To image the meristems, the boxes containing the plants were filled with sterile water and placed under the microscope objective. A 63x 0.95NA Achroplan objective was used for imaging. Z-stacks containing 20 optical sections were acquired using a Zeiss LSM 510 with 543nm laser, 543nm dichroic mirror, 560nm longpass filter, 2μs second scan time per pixel, a resolution of 0.25um(X) by 0.25um(Y) by 1.0um(Z) creating images of 512x512 pixels.

1.2.3 Static Images

For comparison geometric statistics were also measured on a collection of 12 additional images of four different meristems at different time points (approximately 200 cells per image). Arabidopsis seeds of the L-er background were germinated on soil under constant light at room temperature. When the shoots bolted, flowers and flower primordia were dissected from the inflorescence. The meristems were cut from the shoot 1cm below the top and inserted into dishes of solid agar. The meristems were stained with 10uM FM4-64 (Invitrogen) at 4°C for 15 minutes. The meristems were

then washed with distilled water to remove the excess stain and the dishes were filled with distilled water. The same microscope parameters from the time series imaging were used here.

1.2.4 Image Processing

Z-stacks in LSM format were first converted into a TIF series using ImageJ[45] and the LSMToolbox plugin. The functions performed in ImageJ were

1. Import (LSMToolbox plugin)
2. Conversion to 8-bit from 12-bit (Zeiss LSM510 by default captures images in 12-bit)
3. Reverse the image order so the first image is now the last image
4. Save as TIF series

These series of TIF images were then imported into MorphoGraphX. The cell boundaries of the L1 were extracted and segmented using the general methods described previously[44].

Z-stacks in LSM format were first converted into TIF series using ImageJ[45] and the LSMToolbox plugin. These series of TIF images were then imported into MorphoGraphX[44]. The surface of the meristem was extracted using the Closing, Edge_Detect, and Marching_Cubes_Surface functions. The surface mesh was then smoothed and subdivided to around 500,000 vertices. The fluorescent signal from 0 to $3\mu m$ below the surface was projected onto the surface mesh. Segmentation seeds were added by manually clicking in the center of each cell. The surface image was then segmented using the seeds. Cells were created from the segmented boundaries with a minimum of $1\mu m$ between vertices. The full Python code used to automate this method is as follows.

The Python code to generate the 3D mesh was as follows:

```
Stack.Resize_Canvas("Yes","Yes",0,0,20)
Stack.Shift_Stack(0,0,10)
Stack.Average(1,1,1,1)
Stack.Closing(15,15,3)
Stack.Edge_Detect(50000,2,0.3,30000)
Mesh.Marching_Cubes_Surface(5,5000)
Mesh.Smooth_Mesh(1)
Mesh.Subdivide()
```

```
Mesh.Smooth_Mesh(3)
Mesh.Subdivide()
Mesh.Smooth_Mesh(1)
Mesh.Subdivide()
Mesh.Subdivide()
Mesh.Project_Signal("No",1,2,0,50000)
```

Manual seeding of each cell in the image was then performed followed by this Python code

```
Mesh.Segment_Mesh(20000)
count = 0
while count < 2:
    try:
        Mesh.Make_Cells(1)
        break
    except:
        Mesh.Fix_Corners()
        Mesh.Smooth_Mesh(1)
        Mesh.Segment_Mesh(20000)
    count += 1
```

The cells generated by this were exported to a text file for further analysis.

1.2.5 Projection to Local Euclidean Plane

A local Euclidean plane was fit to each cell before division, and to the pair of cells after division. The least squares fit to $z = Ax + By + C$ is described by the normal equations:

$$\begin{bmatrix} \sum x_i^2 & \sum x_i y_i & \sum x_i \\ \sum x_i y_i & \sum y_i^2 & \sum y_i \\ \sum x_i & \sum y_i & n \end{bmatrix} \begin{bmatrix} A \\ B \\ C \end{bmatrix} = \begin{bmatrix} \sum x_i z_i \\ \sum y_i z_i \\ \sum z_i \end{bmatrix} \tag{1.1}$$

Each raw data point (p_i, q_i, r_i) was then projected to the local Euclidean by dropping a perpendicular. Let the nearest point in the projection be (x_i, y_i, z_i), where $z_i = Ax_i + By_i + C$; the coordinates

(x_i, y_i) are found by minimizing the square distance function

$$f = (p_i - x_i)^2 + (q_i - y_i)^2 + (r_i - Ax_i - By_i - C)^2 \tag{1.2}$$

which can be reduced to solving the linear system

$$\begin{bmatrix} A^2+1 & AB \\ AB & B^2+1 \end{bmatrix} \begin{bmatrix} x_i \\ y_i \end{bmatrix} = \begin{bmatrix} Ar_i + p_i - AC \\ Br_i + q_i - BC \end{bmatrix} \tag{1.3}$$

Once the point (x_i, y_i) is known, $z_i = Ax_i + By_i + C$. Both the normal equations for the least squares fit and the projection to the plane are solved using the Mathematica function LinearSolve.

1.2.6 Alignment of Principal Axes

After translation to the local coordinate system each cell is represented by a matrix of data points

$$X = \begin{bmatrix} x_1 - x_c & y_1 - y_c \\ \vdots & \vdots \\ x_n - x_c & y_n - y_c \end{bmatrix} \tag{1.4}$$

where x_c and y_c are the means of the x and y coordinates. The covariance matrix is calculated using the Mathematica function Covariance as

$$M = \frac{1}{n-1} X^T X \tag{1.5}$$

The eigenvectors of this matrix give the principal directions.

Each cell is rotated into a new coordinate system with x' oriented along the eigenvector first principal component (the one with the larger eigenvalue), y' along the second principal component, and oriented so that $x'y'$ points outward from the meristem. The angle of rotation between the before and after coordinate systems is

$$tan\Theta \frac{x'_A \cdot y'_B}{x'_A \cdot x'_B} \tag{1.6}$$

in terms of the unit vectors x'_A,y'_A,x'_B,y'_B in the after and before Euclidean planes. The after-cells can be aligned with the before-cells by rotating through an angle Θ. Finally, each cell is translated

to the center of mass frame[46],

$$x_i = \frac{1}{6}\sum_{j=0}^{n}(x_j + x_{j+1})(x_j y_{j+1} - x_{j+1}y_j) \tag{1.7}$$

$$y_i = \frac{1}{6}\sum_{j=0}^{n}(y_j + y_{j+1})(x_j y_{j+1} - x_{j+1}y_j) \tag{1.8}$$

where the vertices are numbered counter clockwise and vertex 0 is associated with vertex n.

1.3 Results

A total of 207 cell divisions were observed from four Arabidopsis thaliana L-er pUBQ1::2x-tdTomato-29-1 meristems observed from live imaging using laser scanning confocal microscopy. Since the original segmentation was performed in three dimensions the segmentation points for any given cell do not lie precisely in a plane. To perform subsequent analysis, a best fit local Euclidean plane (see Supplemental Information "Projection to Local Euclidean Plane") was found using the method of least squares, and each point was then projected to the local Euclidean plane by dropping the local perpendicular to the plane. The mean offset was $0.07\pm0.05\pm6.2\mu m^2$ (Figure 1.1a). The mean area of the cells before division was $40.0\pm6.2\mu m^2$ (mean $\pm$ standard deviation). The mean area of the daughter cells was $21.0\pm5.5\pm6.2\mu m^2$. Mean cell perimeter before division was $24.9\pm2.1\pm6.2\mu m$, and of the daughter cells was $18.2\pm2.4\mu m$ (Figure 1.1b). The distribution of areas was more symmetric for the parent cell than the daughter cells (skewness of 0.22 vs 0.71). For comparison a study of 4 meristems showed cells areas with mean, sd, skewness. This more closely resembles the skewness in the areas as distributed across the entire SAM (Figure 1.1c) in which the average area was $22.6\pm6.5\mu m^2$.

1.3.1 Cell Expansion and Division in Space and Time

It is known that cells must expand and divide to maintain the amount of tissue in the SAM as groups of cells are incorporated into flower primordia around the periphery and exit the SAM. To quantify this phenomenon we measured the expansion of each cell over each two hour period. The cell expansion occurs in waves as can be seen in Figure 1.2a. This wave phenomenon is also observed in the quantity of divisions over time. Over the observed 38 hours the average expansion rate and

Figure 1.1: (a) Distribution of mean error (mean of the absolute value of perpendicular distance) in fit to local Euclidean. (b) Distribution of parent cell areas before division (white, dashed) and child cell areas after division (gray, solid). (c) Distribution of areas globally across the SAM L1 layer (excluding floral meristems) (4 meristems, 200±26 cells per meristem) and one-sigma errors.

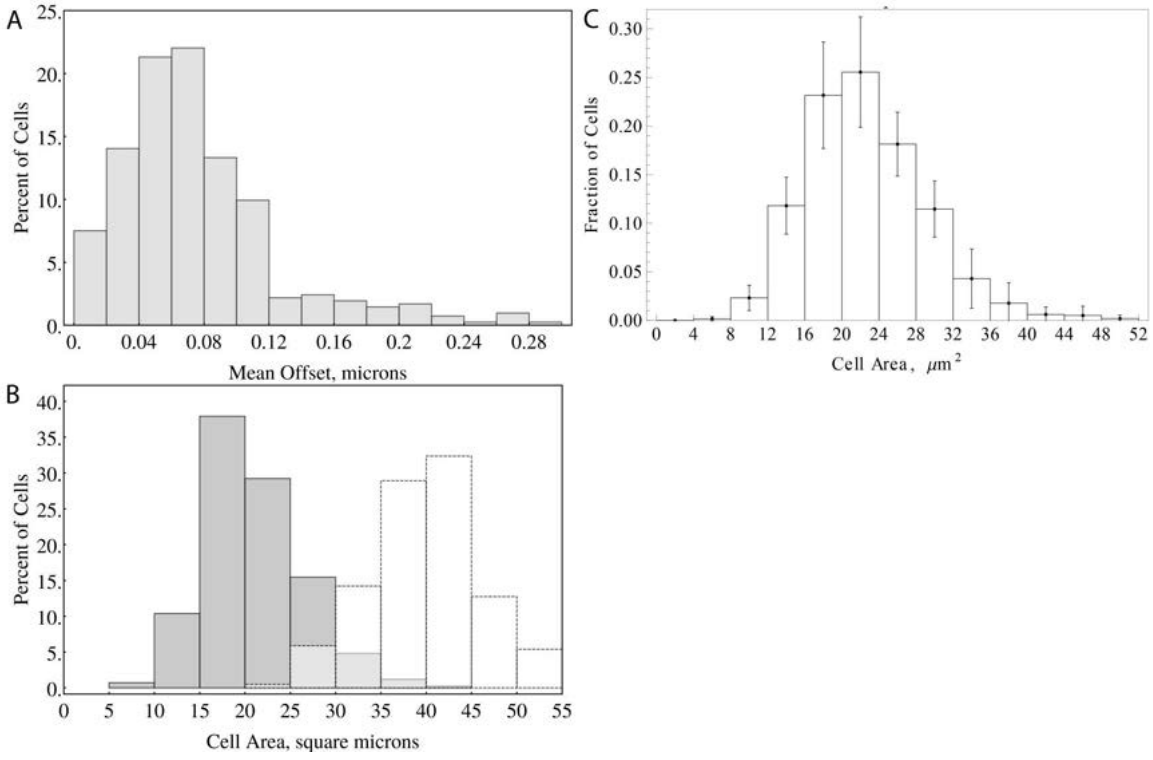

quantity of divisions gradually decreases possibly due to the exposure to laser light, dissection of surrounding flowers, or the repeated submersion in water, all of which effect the health of the plant. It should be noted that while the waves of expansion and division are approximately in phase with each other, the cells that are dividing are not necessarily the same cells that expand the most during any 2 hours.

As shown in Figure 1.2b, cells in the center of the meristem expand very little and in some cases shrink between time points. This phenomenon is observed at all time points and does not fluctuate with the waves of expansion observed elsewhere in the meristem.

To quantify the relation of expansion and division we measured the expansion ratio of cells that divided and cells that did not divide separately, the results of which are shown in the Figure 1.2c. The mean expansion ratio of the 207 dividing cells barely different from that of the nondividing cells: the variance of both populations is too large to differentiate statistically. This suggests that expansion and division are not directly coupled, at least in the two hours prior to division. Given that the cells are all of similar sizes, expansion over the entire cell cycle must be correlated with division.

While rapidly expanding cells have no correlation to dividing cells, there is a bias in the spatial location of the rapidly dividing cells. As seen in the Figure 1.2b, cells towards the top of the meristem are dividing more slowly than those toward the bottom, but there is no clear boundary between rapidly and slowly expanding regions. This phenomenon was observed at all time points.

1.3.2 Analysis of Traditional Heuristics of Cell Division

Many rules about cell division have been reported and widely quoted. Care must be taken in applying these rules as they are all only valid in an approximate sense (as will be shown below) and are often in conflict with one another. Since they are only generally (but not absolutely) valid and are only applicable in the proper context, we refer to them as the heuristics (rather than laws or rules) as they are experience-based guidelines that will often, but not always, work. In addition to the three heuristics that we address below, we also analyzed Hoffmeister's Rule, new walls forming perpendicular to existing walls, and growth immediately after division in the supplementary text (see section "More Heuristics").

Figure 1.2: (a) Solid line indicates the quantity of cells dividing within a given period. Dotted line indicates the mean ratio of cell expansion within a 2 hour period. (b) Heat map on the left shows the amount of cell expansion between the time points at 2 and 4 hours as a ratio. Stars indicate cells that divided during this time period. (c) Histogram on the right shows the mean expansion of cells that divided during any 2h period compared to cells that did not divided.

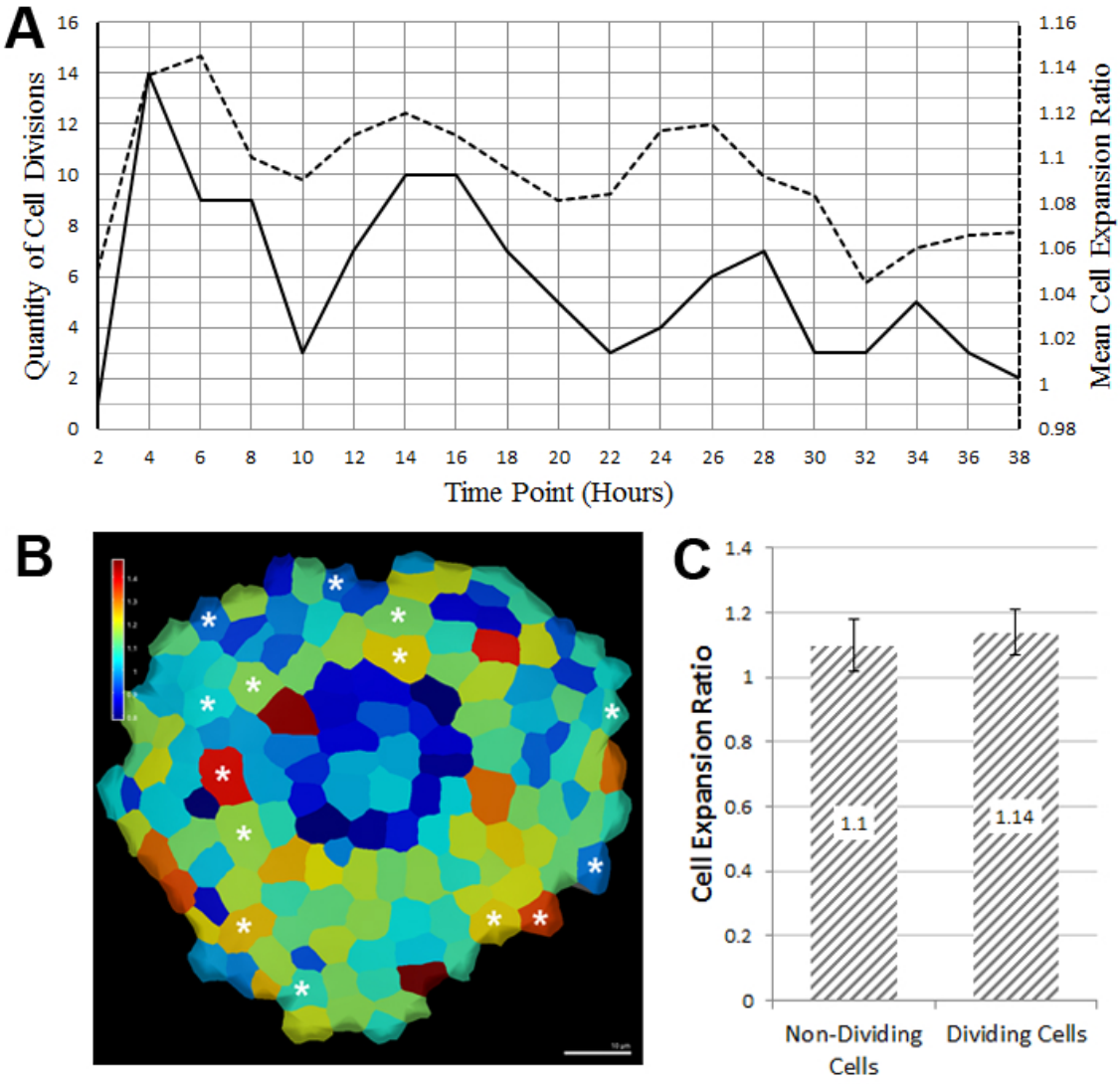

Heuristic 1: The new wall is a minimal surface that divides the mother cell equally

Errera's rule (1888) states that the cell divides along a surface that minimizes the area of the new wall[4]. Errera did not specify the position of the new cell wall (the intersection of the new wall with the cortex). If the wall position is not specified, its minimum area could approach zero in cells of many shapes (conical or spherical for example). To make a predictive model we add as do other modern authors[9, 47, 48, 49] that the division halves the volume of the mother cell. We thus are not testing Errera's actual rule; rather, we are testing the heuristic that modern authors call Errera's rule. For cells in the L1 layer, with uniform depth and anticlinal divisions, we can make a two-dimensional equivalent of this heuristic in which the cell divides along a curve that minimizes the length of the new wall, and that halves the mother cell.

The cells in the 207 cell division sibling pairs ranged from 24 percent to 76 percent of the total area, with a standard deviation of 9.3% within the full range (0.0 to 1.0), as illustrated in Figure 1.3a, which shows the ratio $r = A_i/(A_1 + A_2)$, where A_i is the projected area of the cell in the tangent plane

The divisions that fit this heuristic the worst (bottom 20 percentile) were not evenly distributed throughout the meristem. As it can be seen in Figure 1.3b, in one of the meristems we investigated many of the divisions most poorly predicted occur in the periphery of the meristem. In fact, 72% of the divisions in the bottom 20 percentile occur within three cells of the edge of the meristem. If these uneven divisions are occurring in regions that eventually become primordia, the unevenness of the division might be due to the previously reported phenomenon of a change in the polarity of divisions within founder cells in vegetative meristems [50, 51].

Heuristic 2: The new cell wall passes through the center of the cell

The shortest distance from the new cell wall to the centroid of the cell was determined by (a) fitting a least-squares quadratic to the new cell wall, and (b) finding the minimum distance between the quadratic and the centroid of the combined pair of cells immediately after cell division. The quadratic fit was used to smooth the segmentation which would otherwise be composed of a joined sequence of line segments (Figure 1.4a). To obtain a size-independent (dimensionless) measure, the distance was measured in units of $P/2\pi$, where P is cell perimeter, which would correspond to an effective radius for a spherical cell (illustrated on the right side of figure 5). Some 30%, 50%, and 88% of the cell walls passed within 0.05, 0.1 , and 0.2 effective radii, respectively (Figure 1.5a).

Figure 1.3: (a) Distribution of daughter cells as a fraction of the total area. The total area is defined as the sum of the areas of the two siblings. (b) Division of area of mother cell. (c) How well each division matches the modern interpretation of Errera's rule ranked by percentile and grouped into 10 bins indicated by colors.

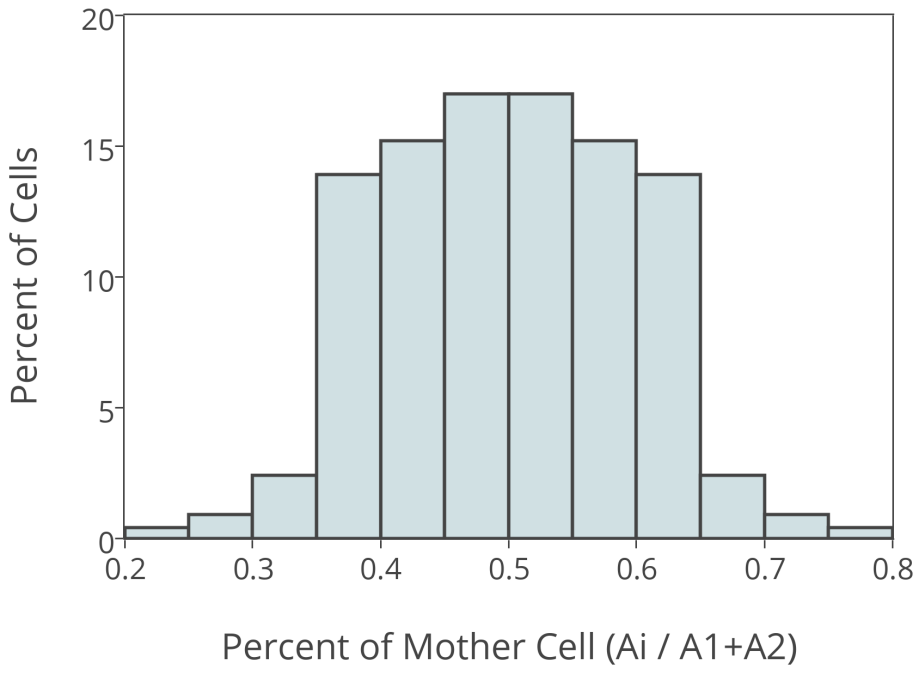

(a)

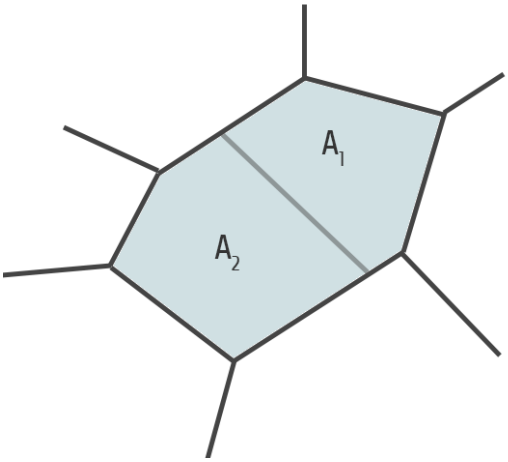

(b)

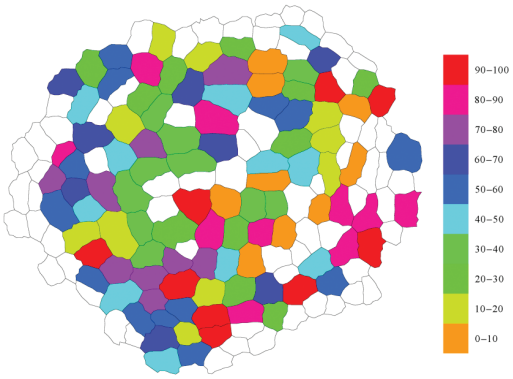

(c)

Figure 1.4: (a) Left: Definition of shortest distance of new cell wall from centroid, for a typical cell. Right: Illustration of the units for values of r=0.05 ,0.1, 0.2, 0.3, and 0.4 for a circular cell. The dashed circles would correspond to a typical cell nucleus that is just skirted by the tangential curved new cell wall. (b) Closest approach of new cell wall to centroid, relative to $r = P/2\pi$, where P is the cell perimeter. Left: distribution; Right: cumulative distribution.

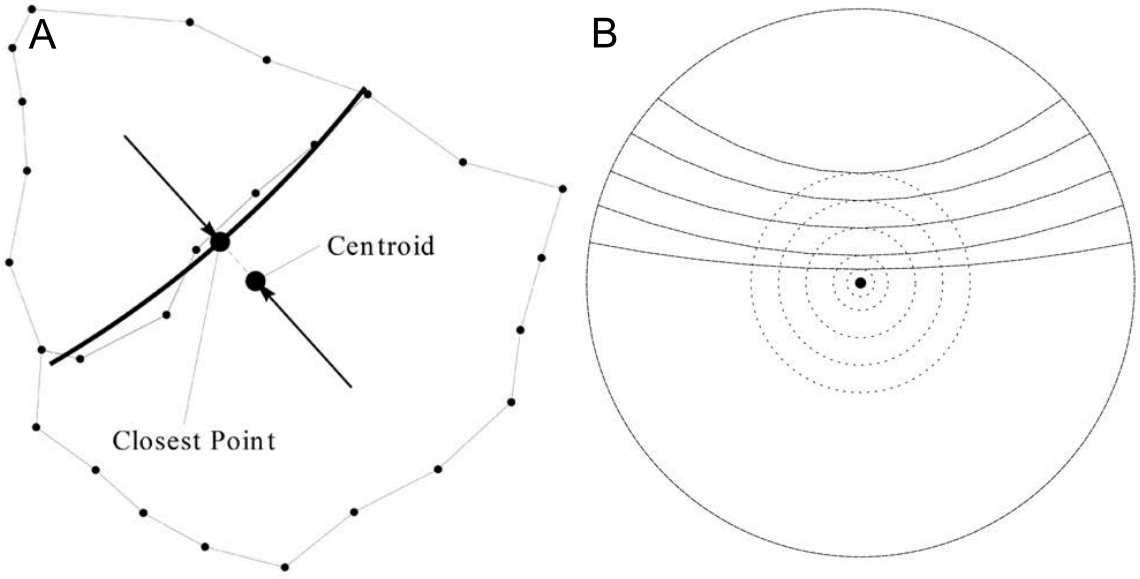

A second measure of how nearly the new cell wall passes through the center of the cell is to measure the angle $\Delta\Theta$ subtended between vectors from the center to the endpoints of the new wall (Fig. 4). In this measure, a straight line wall that passes through the centroid would subtend an angle of 180 degrees. With one exception (at $\Delta\Theta = 88deg$) virtually every cell division subtended an angle of more than 100 deg. As illustrated in Figure 1.5b, 130 deg is exceeded over 90% of the time, 140 deg is exceeded over 80% of the time, 150 deg is exceeded two thirds of the time, and over half the cell division had a central angle exceeding 160 deg, or within 20 degrees of the maximum 180 degrees to make a stright line.

Heuristic 3: The plane of cell division is the shortest path (Soap Bubble Dynamics)

The modern interpretation of Errera's rule (translated to the tangent plane of the L1 layer) suggests that a new cell wall should form along the shortest path that divides the cell evenly. This prediction cannot completely dissociate into two independent heuristics of length minimization and area equalization, in that it minimizes wall length subject to the constraint that the wall divides the cell evenly. However, to assess the significance of a wall shortness constraint we compared

Figure 1.5: (a) Closest approach of new cell wall to centroid relative to $r = P/2\pi$, where P is the cell perimeter. (b) Distribution of new cell wall central angles.

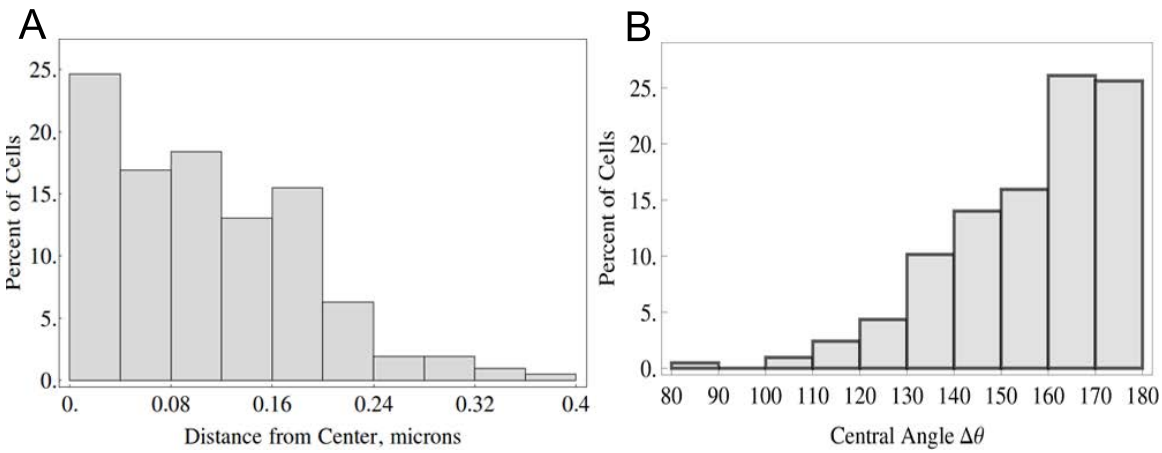

the actual wall lengths to the minimum and maximum diameters of each cell with the statistic $d_{rel} = (d - d_{min})/(d_{max} - d_{min})$. A cell diameter is defined as the length of a line segment passing through the centroid from one cell wall to the opposite cell well. As this line segment is rotated about the centroid its length will change. We call its maximum and minimum values the maximum and minimum diameters. When $d_{rel} = 0$, the wall has the same length as the minimum diameter; when $d_{rel} = 1$, the wall has the same length as the maximum diameter (Figure 1.6). A value of $d_{rel} < 0$ indicates that the actual wall length is shorter than the minimum diameter, because the actual wall does not pass directly through the center but is skewed somewhat. The wall length was defined as the length of the quadratic fit to the new wall (so as to eliminate noise from the image segmentation, see Figure 1.4), and the diameters were defined as the lengths of line segments through the centroid that spanned the entire cell. We found that in 49% of the cell divisions the relative wall length fell within 10% ($|d_{rel}| < 0.1$) of the minimum diameter, and that in 69% of the cell divisions it was within 20% of the minimum diameter. The longest wall had $d_{rel} = 0.67$. More notably, in 76% of the cases, the actual wall length was shorter than the minimum diameter (Figure 1.7).

Heuristic 4: The cell divides perpendicular to the main axis of growth (Hofmeister's Rule)

The difficulty with applying this rule is that it is difficult to calculate the main axis of growth without a fine time-resolution set of live images. Hofmeister (1863) emphasized that the axis of growth is not necessarily the longest diameter of the cell. The instantaneous direction of growth can be defined

Figure 1.6: Definition of cell coordinates in local frame (left) and various parameters used in the definitions of fitness measure (right). The reference axes for definition of angles are the principal components of the segmentation.

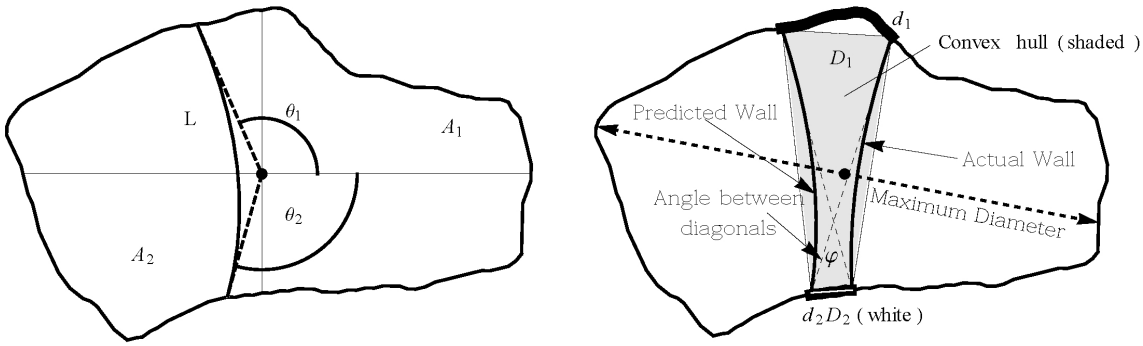

mathematically as the principal axis of the velocities of the vertices (corresponding to the eigenvector with largest eigenvalue of the covariance matrix of the velocities of the vertices)[52]. Alternatively, one might conjecture that since more material will accumulate in the principal direction of growth, that the cell will be extended primarily along that direction. This would imply that the principal axis of the cell (corresponding to the eigenvector with the largest eigenvalue of the covariance matrix of the vertices of the cell, or of the segmentation points, or the principal axis of inertia) should be used to define this main axis of growth. It is challenging to measure the instantaneous direction (despite the algorithm given by [52]) because (1) matching vertices at two different time points assumes that the material at the vertex at one time point should be matched to the vertex at the succeeding time point, and (2) we have observed that cells often shrink (see cell growth heuristic, below) during the time around cell division so it is difficult to assign a meaning to the growth direction in these cells. Because the change in area over the few hours around cell division is very small, and sometimes negative, small errors in segmentation can lead to significant differences in determination of the velocity axis.

Hofmeister's rule (using cell elongation for principal axis) is supported by a change in the distribution of the isoperimetric ratios before and and after cell division. This ratio is $i = 4\pi A^2/P^2$, where A is the area and P is the cell perimeter. It gives a size-independent measure of the elongation of a polygon. A value of $i = 1$ indicates that the cell is nearly circularly shaped; all other closed curves will have a value of less than 1. The further away from 1, the more elongated the cell is. The inequality $4\pi A \leq P^2$ has been attributed to the ancient Greek geometer Zenodorus, in the sense that a circle has greater area than any other regular polygon of equal perimeter. Using the Calculus of Variations it was proven for any closed curve by Jakob Steiner 1836[53]. The typical distribution of

Figure 1.7: Distribution of new wall length. New wall length is expressed as a ratio of the difference between the observed wall length and the minimal wall length to the difference between the maximum wall length and the minimum wall length.

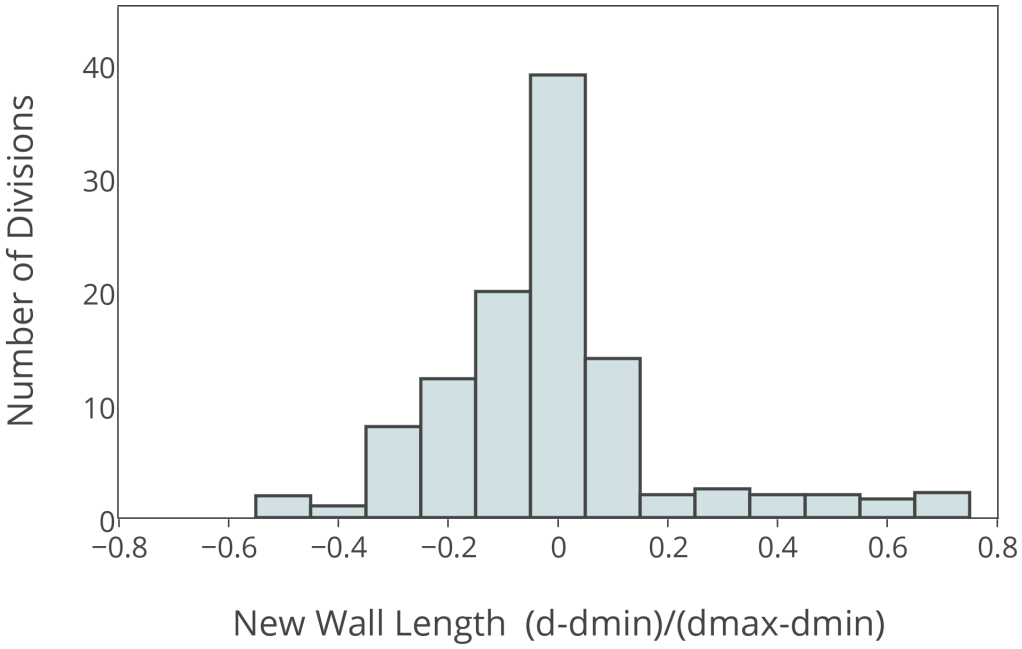

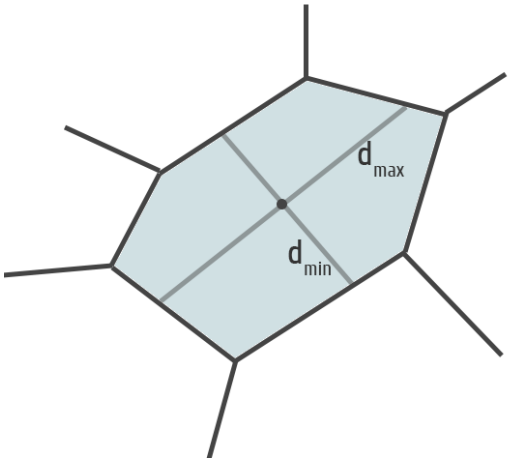

isoperimetric ratio in the L1 layer is illustrated in Figure 1.8a. In Figures 1.8b and 1.8c we compare the isoperimetric ratios before and after cell division. Statistically there is very little difference in the average value of isoperimetric ratio before and after cell division, but the distribution is tighter after division ($i = 0.78 \pm 0.07$) (identical to the global surface average) than before ($i = 0.76 \pm 0.10$). Furthermore, the skewness of the distribution as evident in the overall data is reproduced by the cells after division, but is not as evident in the cells before division. In other words, cells that are about to divide are shaped differently than typical cells. However, this difference does not indicate any particular body shape as the data spread is fairly wide.

The angle between the new cell wall and the principal cell axis is heavily weighted towards perpendicularity (90 degrees), with a differentiation from perpendicular of less than 10 degrees in 30% of the data, less than 20 degrees in 55% of the data, and less than 30 degrees in 75% of the data. This supports the notion that cell elongation should be used to determine new cell wall direction. The actual distribution of these angles is shown in Figure 1.9a. The principal axis is determined as the eigenvector, corresponding to the largest eigenvalue, of the covariance matrix of the projection of the segmentation to the least-squares local Euclidean plane. The direction of the cell wall is found from a least-squares parabolic fit to the new cell wall, as illustrated in Figure 1.9e.

Heuristic 5: The new cell wall forms in a plane that is perpendicular to existing cell walls

To quantify how often the new cell wall forms in a plane perpendicular to existing cell walls the angle between the new cell wall and the existing wall was measured (Figure 1.10). Because the segmentation is pinched in around the intersection, a short arc of the segmentation (up to around 30 degrees central angle in either direction) was fit with a parabola, and the intersection between that parabola and a similar quadratic least squares fit to the new cell wall was used to determine the angle of intersection. The measure used was the smaller of the two interior angles formed by the intersection of the two tangent lines. Some 25% of the intersections were within 5 deg of perpendicular 52% within 10 deg of perpendicular, and 84% within 20 deg of perpendicular when measured in this manner. This is consistent with Sachs' observation, as an emergent property in a statistical sense.

Figure 1.8: (a) Distribution of isoperimetric ratio over 12 timepoints from four different meristems having 200±28 cells in each meristem. (b,c) Distribution of isoperimetric ratios over 207 cell division events for the parents in the last observation before cell division (b) and the first observation after cell division (c). (d) Distribution of angle between new cell wall and normal to principal axis of cell extension (e) Projection of typical segmentation to local Euclidean. The arrow shows the direction of the new cell wall.

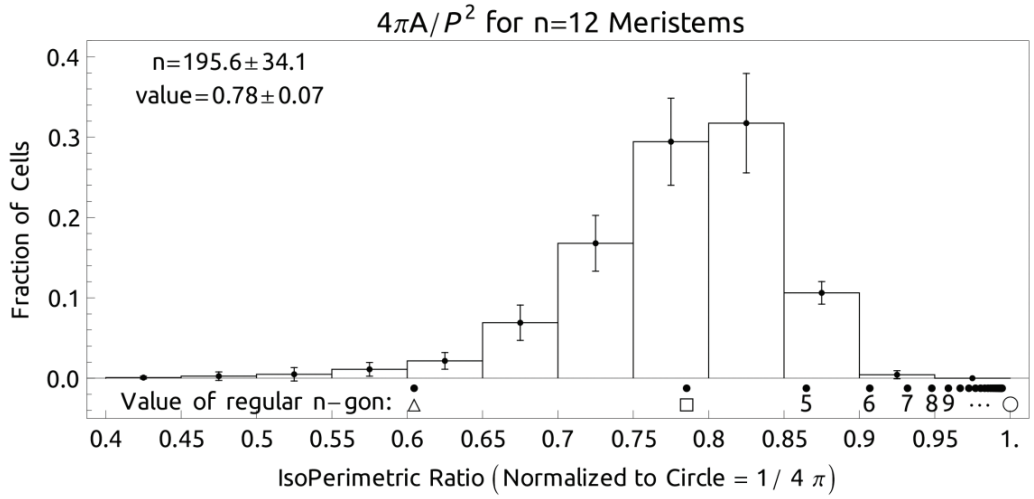

(a)

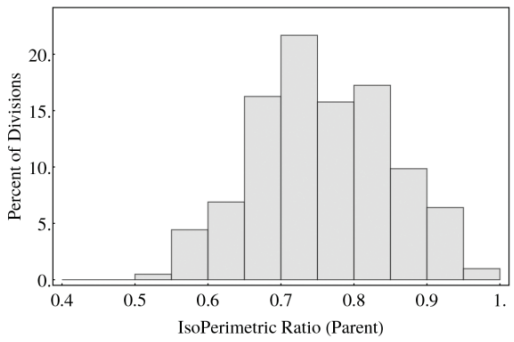

(b)

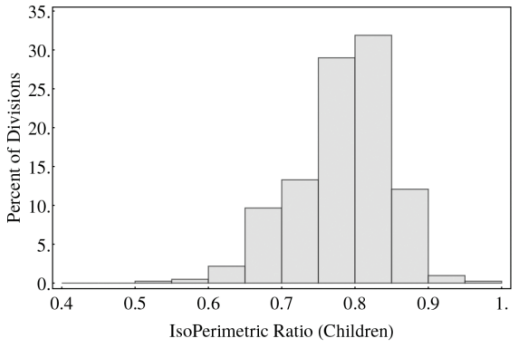

(c)

Figure 1.9: (a) Distribution of angle θ between new cell wall and normal to principal axis of cell elongation. (b) Long arrow indicates primary direction of elongation. Theta is the angle of this direction with respect to the new wall. (c) Least squares fit to vertices.

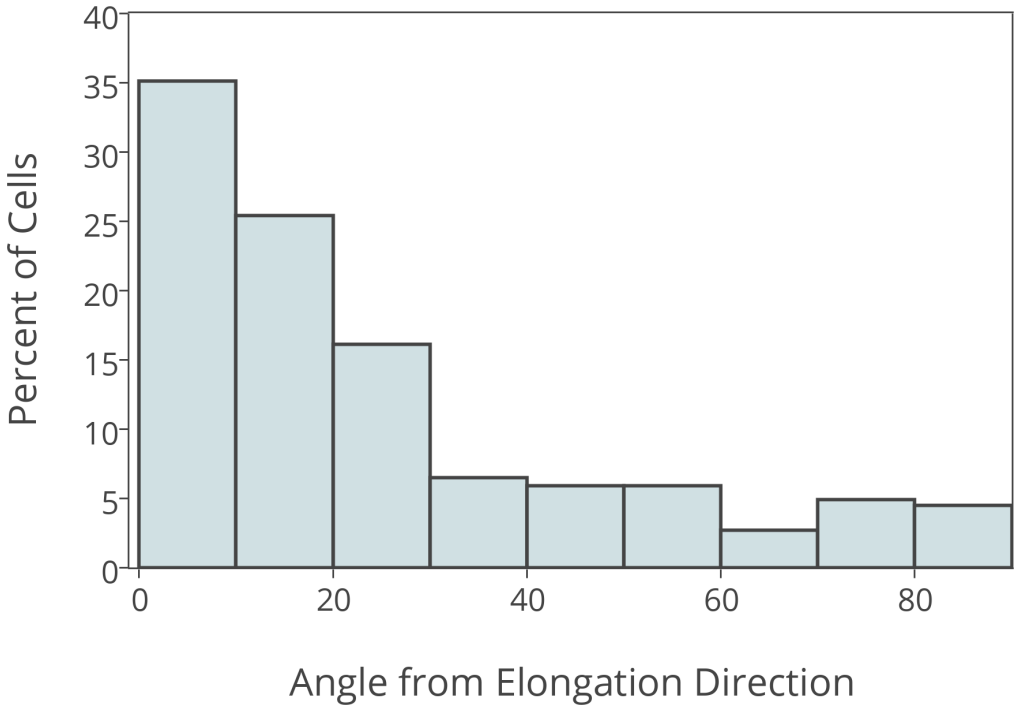

(a)

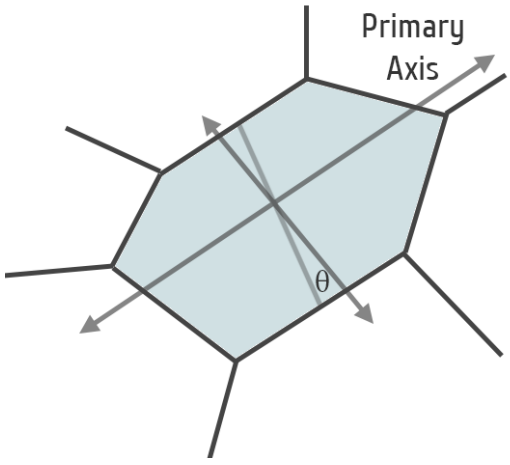

(b)

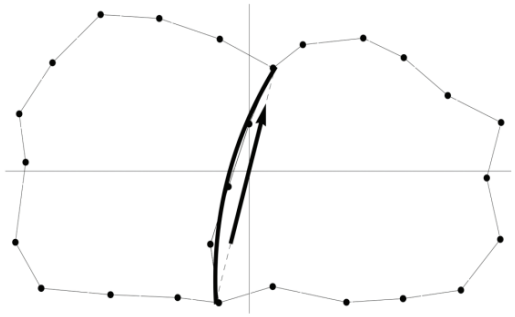

(c)

Figure 1.10: The angle between existing cell wall and new cell wall, degrees. (a) Least-squares quadratics used to calculate angles so as to reduce noise from the segmentation – see dotted line), for a typical cell. (b) Distribution of angle between new wall and existing wall for all cell divisions.

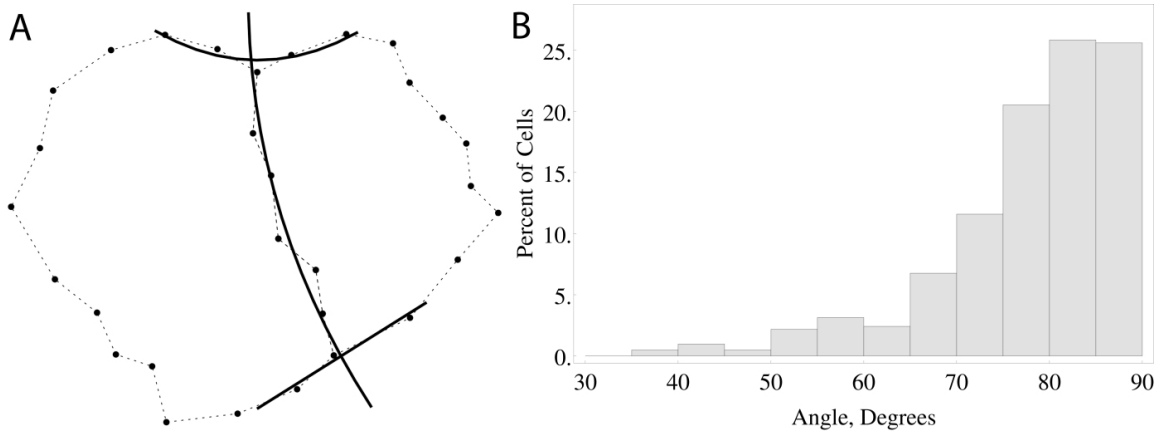

Heuristic 6: The cell continues to grow immediately after cell division

In only 65% of the 207 cell divisions was the area, as measured in the first time point after cell division, greater than the area as measured at the last time point before cell division. The ratio of the area after cell division ($A_{after} = A_1 + A_2$, where A_1 and A_2 are the areas of the sibling pair) to the area before cell division (A_{before}) is illustrated in Figure 1.11. While this may be partially due to an artifact of the image segmentation algorithm (which may favor "pinching" in the corners near the new wall), it may also indicate that perhaps the additional tension added by the new wall may inhibit additional growth for a short period of time after cell division. The various heuristics fall into two categories: those that determine the cell wall completely, and those that put constraints on the optimization process, but do not fully determine wall position on their own.

1.3.3 Model

Four potential functions V_i were defined (see equations (4.5), (1.10), (1.11), (1.12), and (1.13)). For any given weight vector $w = (w_1, w_2, w_3, w_4)$ the cell division potential function $V(\Theta_1, \Theta_2) = \sum_{A,L,g} w_i V_i(\Theta_1, \Theta_2)$ will describe a landscape in (Θ_1, Θ_2) space such that the lowest point of this landscape corresponds to the predicted wall location, with Θ_1 and Θ_2 given the central angles of the two end points of the wall as measured from the cell centroid. When plotted as a function of (Θ_1, Θ_2), this landscape is symmetric about the 45 degree line $\Theta_1 = \Theta_2$ and hence only points above (or below) the line need be considered, as the data are duplicated in both parts of the plot. This landscape may be represented by a contour plot, analogous to a topographic map (see Figure 1.13).

Figure 1.11: Distribution of areas after as compared to before cell division. The ratio of the area after cell division to the area before cell division is shown.

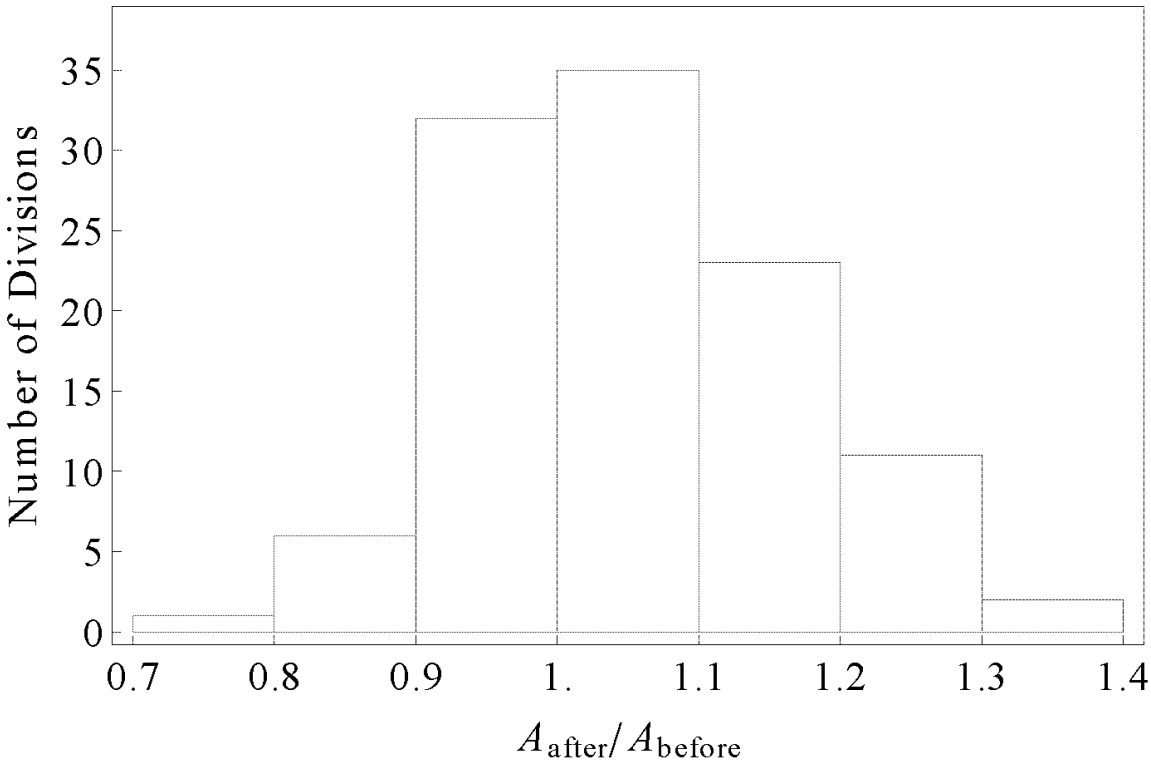

The object of the optimization process is then to find a weight vector that works best in as many cells as possible. Thus the potential is minimized for each cell and each possible weight vector; for each w, the prediction errors are calculated (as a fitness function) for each cell and combined to produce a net fitness for that weight vector.

The cell division model defines a potential function[43, 54]

$$V(\Theta_1, \Theta_2) = \sum_{A,L,e,g} w_i V_i(\Theta_1, \Theta_2) \tag{1.9}$$

where Θ_1 and Θ_2 give the central angles of the end points of the new wall measured from the cell center of mass (Figure 1.6), w is a weight vector, and V_i represents each contributor to cell division.

Four components were include in the sum (4.5): an area potential, a length potential, a perpendicularity potential, and a growth direction potential.

Figure 1.12: (a) Angles θ of new wall from growth direction in 15 degree bins. (b) Relationship between growth axis and plane of cell division, measured by angle θ. (c) θ from all 207 cell divisions.

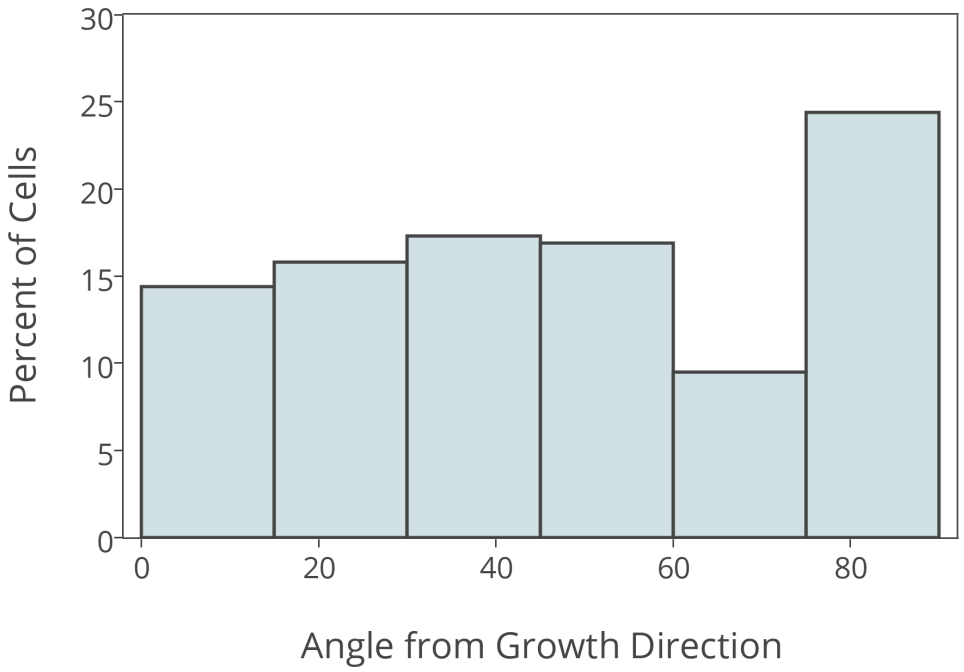

(a)

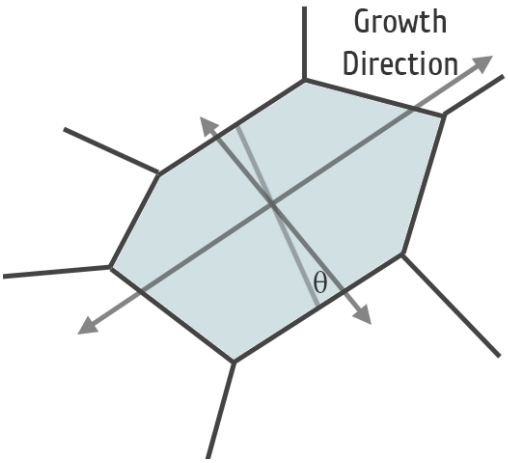

(b)

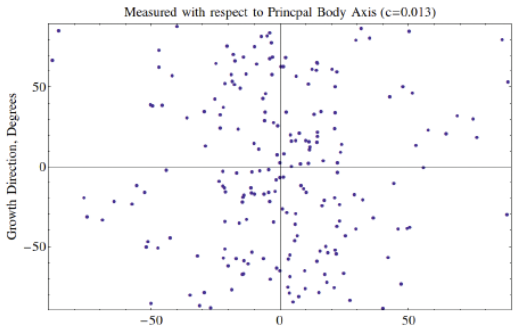

(c)

Figure 1.13: Example of potential function landscape, shown for cell 25 using a weight vector $w = (1, 1, 0, 0)$. Darker regions correspond to higher altitudes and light regions to valleys. The global minimum is show with an open circle and the actual wall endpoints by a dot. The two axes give the angle of Θ_1 and Θ_2 in degrees, and the inset shows an outline of the actual and predicted cell walls.

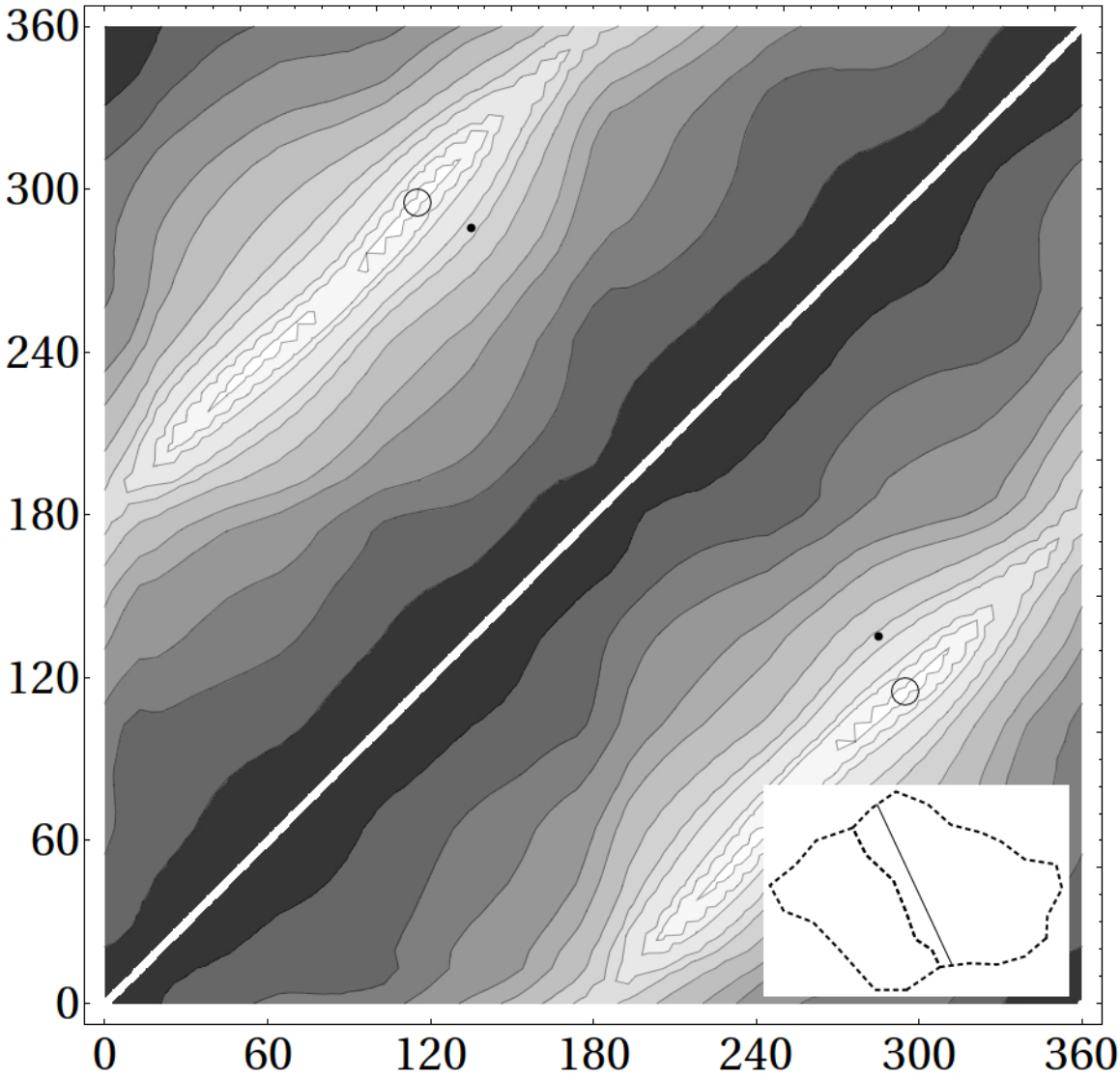

1. The area potential V_A is minimized when the two daughter cells are equal in area:

$$V_A = \left(\frac{A_1 - A_2}{A} \right)^2 \tag{1.10}$$

The function is squared to improve computational stability near the minimum (which would otherwise have a non-differentiable corner there). The disadvantage of this potential is that it does not have a unique global minimum, i.e., any line of cell division will that divides the area in half will give a value of zero. Thus the area potential must be tempered by either an additional potential function (such as the perpendicularity and/or length potential) or an additional heuristic to select the desired minimum value that does not require a unique minimum (e.g, randomly select division direction from amongst all equivalent minima).

2. The length potential V_L is:

$$V_L = \frac{(d - d_{min})^2 + c_L \Delta^2}{(d + d_{min})^2} \tag{1.11}$$

where d is the actual wall length and d_{min} is the minimum length diameter. Thus V_L will be minimized when the cell wall is most closely aligned with the shortest possible diameter.

3. The extension potential V_e is minimized when the new wall is perpendicular to the direction of maximal cell extensionsion potential V_e is minimized when the new wall is perpendicular the direction of maximal cell extension e:

$$V_e = (w \cdot e)^2 + \frac{\varepsilon_g \Delta}{d} \tag{1.12}$$

4. The growth direction parameter V_g is minimized when the new wall is perpendicular to the vector of maximal cell growth g:

$$V_g = (w \cdot g)^2 + \frac{\varepsilon_g \Delta}{d} \tag{1.13}$$

Maximal cell growth direction is calculated using the method described in [52].

The parameter Δ in (1.11), (1.12) and (1.13) gives the shortest distance between the wall and the cell center, with weighting factors ε_e and ε_g. In (1.12) d is the actual wall length. The purpose of the Δ term is to help distinguish between different walls of the same length (for V_L) or direction (for V_g): one that passes closer to the center is more likely than of the same length (or direction) that skirts the edge of the cell; such "skirting" walls would otherwise be predicted by V_L or V_g, especially

in more oblong cells.

The cell division potential was minimized and the fitness function calculated for each of the six methods described in the sup. An average value (corresponding to the fitness function averaged over all 207 cell divisions) was assigned to each value of the weight vectors. Since only the direction of the weight vector, and not its actual length, is important in finding the minimum value, the four component weight vector $w = (w_1, w_2, w_3, w_4)$ can be represented by a unit vector in the same direction; e.g., the weight vector $(1, 1, 0, 0)$ is completely equivalent to a weight vector $(\sqrt{2}, \sqrt{2}, 0, 0)$. The four dimensional weights were found by taking three dimensional slices along two planes, holding parameter three fixed and holding parameter four fixed. With this constraint, each three component weight vectors in a slice can be described by two angles (α, δ), giving the azimuth and elevation in w space, where $w_x = cos\delta cos\alpha$, $w_y = cos\delta sin\alpha$, and $w_z = sin\delta$. A global search of weight vector space was then performed at approximately 3 degree increments (620 values) to obtain a coarse description of the fitness. A spatial resolution of 3 degrees was also used. For computational efficiency only cell walls with a minimum central angle of 90 degrees were considered during the optimization (as suggested by Figure 1.4). Predictions were made using the pre-division observations ("before" data) obtained at the start of a two hour window during which cell division took place, and evaluated in comparison to the observed location of the cell wall as determined from post-division observations ("after" data) obtained at the end of the same window. For comparison, a second set of predictions were calculated using only the "after" data ("hindsight" predictions). In the hindsight predictions the outer boundary of the pair of daughter cells was used to represent the pre-division cell wall.

1.3.4 Fitness Functions

We asked the question whether any weight vector w could be found such that $V(\Theta_1, \Theta_2)$ is minimized when the predicted angle pair matches the actual cell division plane. To determine the weights we performed a coarse global search on the first quadrant of the global hyper-sphere $|w| = 1$. For each w value, the location of the minimum potential in (Θ_1, Θ_2)-space was determined and subjected to a fitness measure. For any given cell i, the following fitness measures were considered:

1. Error in distance between endpoints of actual and predicted wall, as measured along the circumferential path of the boundary, measured relative to the maximal cell diameter:

$$f_{i,boundary} = \sum_{j=1}^{n} \frac{d_1 + d_2}{d} \tag{1.14}$$

2. Actual distance between endpoints of actual and predicted cell wall, relative to maximal cell diameter:

$$f_{i,boundary} = \sum_{j=1}^{n} \frac{d_1 + d_2}{d} \tag{1.15}$$

3. Area of the convex hull of the four endpoints of the actual and predicted cell wall, relative to the total cell area:

$$f_{i,area} = \frac{A_{convexhull}}{A_{cell}} \tag{1.16}$$

4. Smaller of the two angles between the diagonals of the convex hull of the four endpoints, divided by 90 degrees; if on of the endpoints falls inside the convex hull of the other three points, this devolves to the angle between the actual and predicted cell wall

$$f_{i,angle} = \frac{\varphi}{90} \tag{1.17}$$

5. Relative Euclidean distance in angle space; if the actual and predicted walls have endpoints at central angles $(\Theta_{A,1}, \Theta_{A,2})$ and $(\Theta_{A,1}, \Theta_{A,2})$ measured in degrees, then

$$f_{i,\Theta} = \frac{\sqrt{(\Theta_{A,1} - \Theta_{P,1})^2 + (\Theta_{A,2} - \Theta_{P,2})^2}}{90\sqrt{2}} \tag{1.18}$$

6. The Hausdorff distance between the actual and predicted cell division line. The Hausdorff distance between two sets gives the maximum distance in the first set to the nearest point in the second set. Hausdorff distances were estimated numerically by computing distances at 100 equally spaced points along each wall.

Each fitness measure was averaged over all 207 cell division. The results were sorted by fitness (lower is better) and clustered by location in -space to find a best fit vector, which could be used to, for example, to predict cell division, as implemented in Cellzilla.

1.3.5 Cellzilla Growth Model

Cell growth is described by a Hooke's law spring potential $\phi = \frac{1}{2} \sum k_{ij}(|\Delta x_{ij}| - \ell_{ij})^2$ applied to each pair of vertices, and summed over all adjacent vertices. Here k_{ij} is a constant assigned to the wall joining vertex i with vertex j, and Δx_{ij} is an extension or compression of a virtual spring beyond its equilibrium length ℓ_{ij}. The net force will pull vertex v_i towards v_j if if the spring is extended,

and push the vertices apart if the spring is compressed, as described below by (1.19). Pressure is described as a force per unit wall length, so that it can be applied equally at each vertex.

Cellzilla is a two-dimensional tissue growth simulation extension for Cellerator[55]. Each cell is described as a single polygonal compartment. Growth occurs via dynamics assigned to each vertex v_i as

$$\frac{dv_i}{dt} = -\sum_j k_{ij}\left(\frac{v_i - v_j}{|v_i - v_j|}\right)(|v_i - v_j| - \ell_{ij}) + \frac{1}{2}P\sum_j\sum_a n_{ij,a}|v_i - v_j| \tag{1.19}$$

where the sums over j are over all vertices that are connected to i and the sum over a is over all cells that abut the edge connecting vertices i and j. The first term describes a weak spring dynamics, where k_{ij} and ℓ_{ij} are the spring relaxation constant and resting length for the edge connecting vertices i and j. The second term describes an internal turgor pressure P in each cell that is applied normal to the cell wall (normal vector $n_{ij,a}$ and divided equally between the vertices; similar dynamics have been used by others, e.g.[56, 57]). Isotropic linear growth is described by increasing the resting length of cells:

$$\frac{\ell_{ij}}{dt} = \mu\Theta\left(|v_i - v_j| - \ell_{ij}\right) \tag{1.20}$$

where

$$\Theta(x) = \frac{x + |x|}{2} \tag{1.21}$$

Cell division occurs when the cell passes a mass threshold. Each cell is randomly assigned a unique mass threshold at creation, with the population of thresholds distributed normally. The placement of the new cell wall may be assigned either by the modern interpretation of Errera's rule or a potential model as described elsewhere in the paper.

We optimized a the third component of the weight vector for growth direction rather than the geometrical prinicipal axis using a subset of cell divisions (14) using the protocol of Goodall and Green[52] to determine cell growth direction over a two hour period. The optimal weight vector shifted to w=(0.9, 0.4, 0). There was very little difference as either of the first two components (area and length) are varied. However, optimality rapidly decreases as the third component becomes non-zero. This would indicate that the actual instantanteous direction of growth (as measured over a two-hour period) is not a significant predictor of cell division.

The minimum fitness results were clustered around a weight vector of $w = (0.68, 0.73, 0, 0)$, where the three values represent the relative importance of area equalization, length minimization, and perpendicularity to cell elongation (Figure 1.14). Variations in the first component have very little

Figure 1.14: Result of optimization of potential.

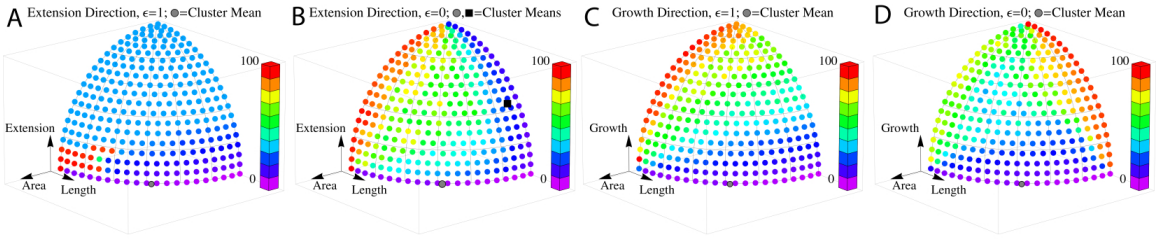

effect, except as $w_1 \to 1$, where it becomes rapidly worse for $w_1/w_2 > 19$. The fitness decreases gradually as w_3 increases from zero. There were no significant differences between the different types of fitness measure. All of our fits indicate that the third component in w is zero. This indicates that neither geometrical elongation nor instantaneous direction of growth (as measured over a two-hour period) are significant predictors of cell division.

When the constants c_1 and c_2 were relaxed to zero in (11) and (12) the minimum moved to $w = (1, 0.6, 0)$, with the valley of minimums spread widely along the equator (Figure 1.14c), indicating that almost any combination of area equalization and and length minimization will work so long as both factors are taken into account (i.e., avoiding the end-points of pure-length and pure-area). In the first set of optimization runs, area equalization was not so important because the length-potential forced the new wall to pass near the center. When this restriction is removed, a delicate balancing between length-minimization and area-equalization is required to compensate for this. The direction of cell elongation did not appear to be a significant driving factor in either situation; in fact, incorporation of this factor with $c_2 = 0$ seemed to make matters worse.

This result would, indeed, suggest that when the different predictors are dissociated in this manner, that the best predictor is the shortest length wall that passes near the center. This prediction is very similar to the modern interpretation of Errera's rule that the wall will form in the shortest path that divides the cell in half. To compare these statements, the predicted wall location according to this rule were computed for all 207 cell divisions. The distribution of fitnesses for a potential function minimization with $w = (0.68, 0.73, 0, 0)$ were slightly better than for the modern interpretation of Errera's rule (Figure 1.16). Thirteen of the 14 worst cases were the same cells for both methods. Visually there is very little difference between the two methods of prediction. Using a distance fitness measure, the potential method gave a better fit in 68 of the 207 cell division, the modern interpretation of Errera's method in 40 cases, and both had identical fitnesses in two cases. In the hindsight model the numbers were 36 (Errera), 2 (tie), and 72 (potential) (see supplemental material

Figure 1.15: Simulated z-projection of meristem grown from a single cell in Cellzilla after 1000 cell divisions. (a) The modern interpretation of Errera's Rule used for cell division. (b) Optimized potential model using $w = (0.1, 1, 0)$ (area, length, cell extension).

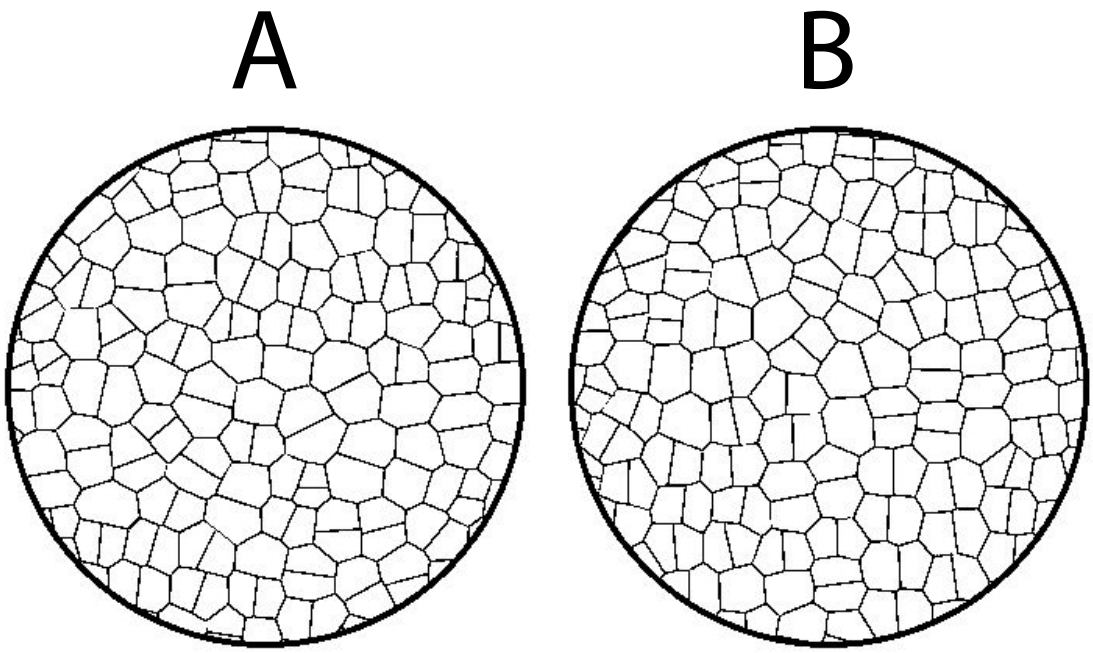

items 1 - 3).

Simulation results for both the modern interpretation of Errera's model and the optimized potential model are illustrated in Figure 1.15 after 1000 cell division have occurred (see also the movies in supplemental material 4 and 5). The tissues were grown in-silico from single quadrilateral cells and projected onto a parabolic surface. The resulting cell division patterns in both cases are evocative of observed data.

Cell Division is a Boltzmann Distribution

Following the work of Besson and Dumais[9] we evaluated the hypothesis that selection of cell division surface may follow a Boltzmann distribution

$$Pr_{surface} = \frac{exp(-\beta \Delta V_{surface})}{Z(\beta)} \tag{1.22}$$

where $X(\beta)$ normalizes the distribution and beta is the inverse of temperature) in a phenomenological potential function, rather than actually minimizing the potential function for each cell all

the time. In the limit of zero temperature such a model is equivalent to minimizing the potential; nonzero temperatures (finite betas) record departures from minimality. In this analysis we applied the prior authors' concept of a thermodynamic model to our data; we applied their model to our data to see how their potential function $\Delta V = lp$ compared with ours (4.5) in a thermodynamic analysis. We evaluated the Besson & Dumais model against our data, as our model uses straight lines for cell division and theirs uses arcs of circles. When we evaluated their model we used arcs of circles. Figure 1.17 supports this hypothesis with quantitative evidence from SAM cell images, both for our potential function (Equation (4.5) and Figure 1.17a) and for the Besson-Dumais potential function (Supplement Equation (1.13) and Figure 1.17a), though with a substantially lower effective temperature for our proposed potential function.

1.3.6 Model Predictions

The minimum fitness results were clustered around a weight vector of $w = (0.68, 0.73, 0, 0)$, where the four values represent the relative importance of area equalization, length minimization, perpendicularity to cell elongation and perpendicularity to growth direction (Figure 1.14). Variations in the first component have very little effect,except as $w_1 \to 1$, where it becomes rapidly worse for $w_1/w_2 > 19$. The fitness decreases gradually as w_3 increases from zero. There were no significant differences between the different types of fitness measure. All of our fits in the primary cluster indicate that the third component in w is zero. This indicates that neither geometrical elongation nor instantaneous direction of growth (as measured over a two-hour period) are significant predictors of cell division. A second cluster of minima occurs around $(0.02, 0.81, 0.58, 0)$ in the case where $c_p = 0$ in (1.12) corresponding to cell extension. No significant change was observed in changing the constant c_p corresponding to cell growth direction, nor with any change with any change observed when the constant c_L in (1.11) was changed.

This result would, indeed, suggest that when the different predictors are dissociated in this manner, that the best predictor is the shortest length wall that passes near the center. This prediction is very similar to the modern interpretation of Errera's rule that the wall will form in the shortest path that divides the cell in half. To compare these statements, the predicted wall location according to this rule were computed for all 207 cell divisions. The distribution of fitnesses for a potential function minimization with $w = (0.68, 0.73, 0, 0)$ was slightly better than for the modern interpretation of Errera's rule (Figure 1.16). Thirteen of the 14 worst cases were the same cells for both methods.

Figure 1.16: Comparison of predictions between the length-minimization potential, and the Besson-Dumais model. Dotted lines: actual new wall. Solid lines: predicted new wall.

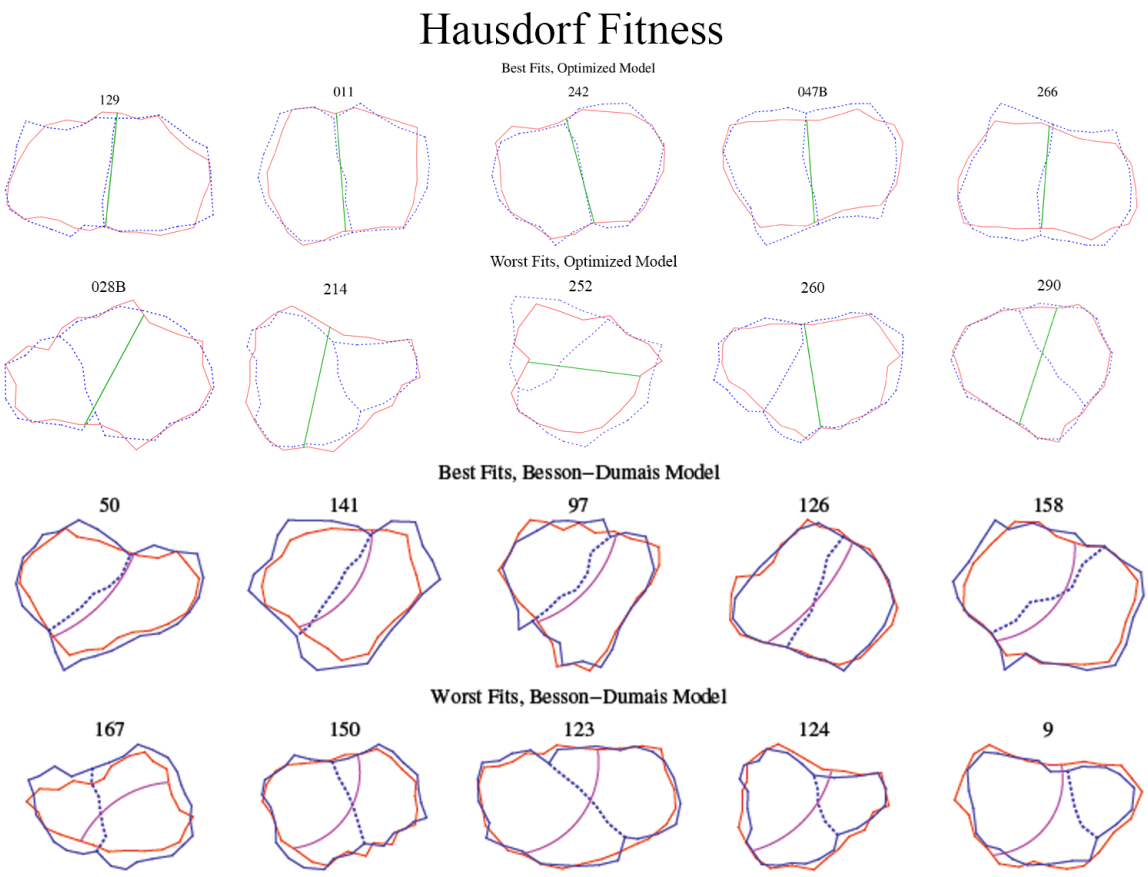

Visually there is very little difference between the two methods of prediction. Using a distance fitness measure, the potential method gave a better fit in 68 of the 207 cell division, the modern interpretation of Errera's method in 40 cases, and both had identical fitnesses in two cases. In the hindsight model the numbers were 36 (Errera) 2 (tie), and 72 (potential).

Simulation results for both the modern interpretation of Errera's model and the optimized potential model are illustrated in Figure 1.15 after 1000 cell division have occurred (see also the movies in supplemental material 4 and 5). The tissues were grown in-silico from single quadrilateral cells and projected onto a parabolic surface. The resulting cell division patterns in both cases are evocative of observed data.

1.3.7 Comparison to the Besson-Dumais Model

We evaluated the Besson-Dumais model on our data set by calculating the most likely wall location from among all allowed wall locations, where a wall location was allowed if its endpoints subtend a minimum central angle, as measured from the cell centroid, of 135 degrees (a restriction we have justified by the histogram in Figure 1.8c). In Figure 1.17 we compare the results of our model with the Besson-Dumais model. In order to make a valid comparison we computed the loghistogram of $|\Delta V|$, the difference between the predicted and actual potential used by the cell, for each model. For our model we plotted the log-histogram of $|\Delta V|$, where V is computer by (4.5) and for the Besson-Dumais model we plotted the log-histogram of $|\Delta V|$ where $V = l/p$. In each case we computed the weighted least squares fit:

$$\log N = a|\Delta V| + b \tag{1.23}$$

where the slope b and intercept a are solutions of the normal equations

$$\begin{bmatrix} \langle|\Delta V|^2\rangle & |\Delta V| \\ |\Delta V| & 1 \end{bmatrix} \begin{bmatrix} a \\ b \end{bmatrix} = \begin{bmatrix} \angle|\delta V| \log N\rangle \\ \langle \log N\rangle \end{bmatrix} \tag{1.24}$$

The expectations are computed by defining a normalized weight vector $w = \frac{1}{N}n$, where n is the vector of counts in each bin, and $N = \sum n_i$. Then

$$\langle|\Delta V|\rangle = \sum w_i|\Delta V|_i \tag{1.25}$$

$$\langle|\Delta V|\rangle = \sum w_i|\Delta V|_i^2 \tag{1.26}$$

$$\langle|\Delta V| \log N\rangle = \sum w_i|\Delta V|_i \log n_i \tag{1.27}$$

$$\langle|\log N|\rangle = \sum w_i \log n_i \tag{1.28}$$

The negative of the slope corresponds to inverse temperature, the parameter β in the Besson-Dumais model. As can be seen the resulting distributions are similar. The corresponding fits (the straight lines in Figures 1.17 A and B) have slope -10.4 (Besson-Dumais) and -62.1 (Potential Model). When a similar least squares fit was computed without the weighting the corresponding slopes were -9.0

(Besson-Dumais) and -45.9 (Potential Model). By comparison, the similar empirical fits by Besson-Dumais of a Boltzmann distribution with energy function $V_{BD} = l/p$, on their data in their figure 6B for four species (Coleochaete, Microsorum, Dionaea, and Zinnia) resulted in a slope of with a "universal" or cross-species best fit slope β of 20.6. This difference of results for the potential function V_{BD} may be accounted for by the different ways we and Besson-Dumais use the same potential function. Besson-Dumais consider just a few cell division surfaces between pairs of cell sides, allowing arcs; we consider straight lines, specified by two continuous intersection angles finely discretized into 10000 angle pairs, and restricted by central angle as above. Thus, in the direct comparisons that have been made, we find a substantially lower effective temperature $1/\beta$ and thus substantially less randomness, using our proposed potential function rather than that of Besson-Dumais.

1.4 Discussion

Previous work in this field has shown that rules must exist to control the positioning of new cell walls in the meristem in order to produce the patterns (size, shape, and connectedness) that are observed[43, 56]. Here we determined that the rules are not simple, and in fact the rules seem to be different depending on the location in the meristem. This might be a result of flower founder cells changing their "preferred" division polarity prior to the rapid growth characteristic of flower primordia. This is similar to the observation in vegetative meristems of pea plants where leaf founder cells often divide periclinally (parallel to the surface of the meristem) about one half plastochron before primordial growth where non-founder cells would usually divide anticlinally (perpendicular to the surface)[58, 59]. This is different than the phenomenon observed in Arabidopsis inflorescence meristems where periclinal divisions are not observed, but similar in that the divisions which don't abide by the modern interpretation of Errera's rule or our potential minimization rule are found preferentially near the edge, possibly in regions of flower founder cells. One explanation for the deviation from the rules near the perimeter of the meristem is that it helps make the elongated cells commonly observed in the boundary region of new primordia.

Explanations for these rules get more complicated when we consider the underlying mechanisms controlling plant cell divisions. Prior to cell division actin filaments and microtubules expand outward from the nuclear to the cellular membrane, in a pattern that resembles a concentric spoked wheel[60]. Following this, the region defined by the ends of the spokes develops the preprophase

Figure 1.17: Comparison of our model with that of Besson and Dumais [9]. Histograms show $log|\Delta V|$, the difference between the predicted and actual potential used by the cell, for each model. The negative of the slope corresponds to inverse temperature, and the parameter β in the Besson-Dumais model.

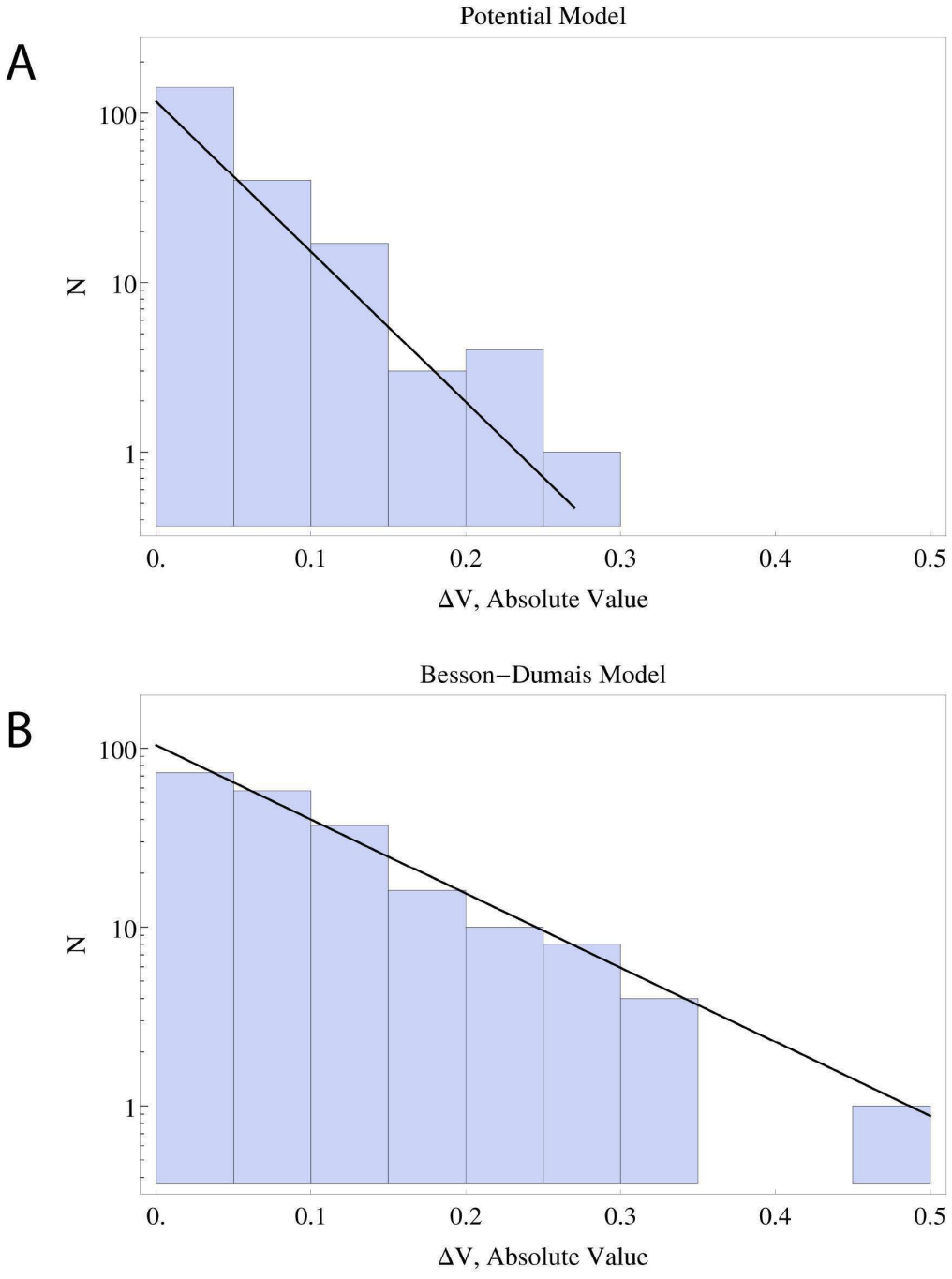

band of microtubules, which defines the position of the new cell wall. If the shape of the spoked wheel is then perturbed somewhat from circular, and the inner wheel is perturbed somewhat from the center of mass, we have an oblong cell with an off-center nucleus. Presuming that multiple spokes grow outward from the inner wheel, starting at the same time, the first spokes to reach the outer wheel will be the ones that have to travel the shortest distance. Reaching the outer membrane will induce a change in tensile forces and this could be transmitted as a signal back to the nuclear end of the spoke. In this model a new cell wall would be represented by the first two spokes to reach the outer wall, together with a collection of filaments tangent to inner circle (e.g., near the nuclear membrane) that connect them. At this point the full PPB has not coalesced yet and the filaments of the new proto-wall are free to increase their tension, forming into a more smoothly aligned curve that connects the two endpoints, perhaps tangent to the inner circle or even forming a straight line.

This argument would support a model in which shortest distance paths that pass close to the cell nucleus dominate (as suggested by a weight vector heavily dominated by the length potential). Since lines that pass through the center of the cell will, on the average, divide the cell in half, a rule stating that a new wall be the shortest path that divides the cell in half will emerge as a consequence. Furthermore, since the shortest distance from a point (e.g., the nucleus) to a line (e.g., the outer cell wall) is along a perpendicular path, Sachs' observation that new walls are perpendicular to existing walls and daughter cells are equal in volume[13] will also emerge. Finally, since the principal axis of elongation is, by definition, the longest axis of the cell, there paths will cluster about the shortest path normal to the principal axis that passes through (or nearly through) the cell center. Thus Hofmeister's Rule[11] is also emergent.

Nevertheless, the modern interpretation of Errera's rule is a poor predictor in a number of cases. In many of these cases the actual wall forms closer to the longest wall that divides the cell in half rather than the shortest. This may indicate that additional dynamic forces are involved in these cells that are not accounted for by a minimum length heuristic.

The model of shortest path that passes nearly through the cell center thus eliminates the need for the cellular machinery to somehow "sense" either the cellular orientation (elongation) or direction of growth. That biomechanical forces could affect the growth of the microtubules is nevertheless likely, perhaps changing their growth rate or causing a preferential growth direction. This could possibly explain the cases in which none of the traditional rules are followed.

It should be noted that this study only considered the first layer of cells in the meristem which have a uniform thickness and divide only periclinally. More could be learned about the mechanisms of cell division if divisions were observed in tissues that divide in all directions and the images were processed in 4D (3D z-stacks over time) using the methods of Fernandez et. al., for example[60]. Such a study would be indicative of how universal or narrow our rules are throughout plant tissues in general. Additional studies should also look at how cell divisions planes are affected by mechanical perturbations of the tissue prior to division.

References

[1] Ian J Furner and Joanne E Pumfrey. "Cell fate in the shoot apical meristem of Arabidopsis thaliana". In: *Development* 764 (1992), pp. 755–764.

[2] Jan Traas and Teva Vernoux. "The shoot apical meristem: the dynamics of a stable structure." In: *Philosophical Transactions of the Royal Society of London. Series B, Biological Sciences* 357.1422 (June 2002), pp. 737–47. ISSN: 0962-8436.

[3] S Satina, AF Blakeslee, and Amos G Avery. *Demonstration of the Three Germ Layers in the Shoot Apex of Datura by Means of Induced Polyploidy Periclinal Chimaeras*. 1940.

[4] L Errera. "Über Zellformen und Seifenblasen". In: *Botanisches Centralblatt* 34 (1888), pp. 395–398.

[5] Frederic T. Lewis. "The effect of cell division on the shape and size of hexagonal cells". In: *The Anatomical Record* 33.5 (Sept. 1926), pp. 331–355. ISSN: 0003-276X.

[6] D'Arcy Wentworth Thompson. *On Growth and Form*. Cambridge University Press, 1992, p. 345. ISBN: 0521437768.

[7] E B Matzke. "The Three-Dimensional Shapes of Bubbles in Foams." In: *Proceedings of the National Academy of Sciences of the United States of America* 31.9 (Sept. 1945), pp. 281–9. ISSN: 0027-8424.

[8] Clive W. Lloyd. "How does the cytoskeleton read the laws of geometry in aligning the division plane of plant cells?" In: *Development* 113.Supplement_1 (Jan. 1991), pp. 55–65.

[9] Sébastien Besson and Jacques Dumais. "Universal rule for the symmetric division of plant cells." In: *Proceedings of the National Academy of Sciences of the United States of America* 108.15 (May 2011), pp. 6294–9. ISSN: 1091-6490.

[10] Laurie G Smith. "Division Plane Determination in Plant Cells". In: *Plant Physiology*. Ed. by Lincoln Taiz and Eduardo Zeiger. 5th ed. Sinauer Associates, 2006. Chap. 16.1.

[11] W Hofmeister. "Zusatze und berichtigungen zu den 1851 veröffentlichen untersuchungen der entwicklung höherer kryptogamen". In: *Jahrbucher fur Wissenschaft und Botanik* 3 (1863), pp. 259–293.

[12] T M Lynch and P M Lintilhac. "Mechanical signals in plant development: a new method for single cell studies." In: *Developmental Biology* 181.2 (Jan. 1997), pp. 246–56. ISSN: 0012-1606.

[13] J Sachs. “Uber die Anordnung der Zellen in jungsten Pflanzentheilen”. In: *Arbeiten des Botanisches Institut Wurzburg* 2 (1878), pp. 46–104.

[14] Nicolas Minc and Matthieu Piel. “Predicting division plane position and orientation.” In: *Trends in Cell Biology* 22.4 (Apr. 2012), pp. 193–200. ISSN: 1879-3088.

[15] D J Flanders et al. “Nucleus-associated microtubules help determine the division plane of plant epidermal cells: avoidance of four-way junctions and the role of cell geometry.” In: *The Journal of cell biology* 110.4 (Apr. 1990), pp. 1111–22. ISSN: 0021-9525.

[16] Edmund W Sinnott and Robert Bloch. “The Relative Position of Cell Walls in Developing Plant Tissues”. In: *American Journal of Botany* 28.7 (1941), pp. 607–617.

[17] D.J Chadi. “Energy-minimization approach to the atomic geometry of semiconductor surfaces”. In: *Surface Science* 299-300 (Jan. 1994), pp. 311–318. ISSN: 00396028.

[18] H.G. Timberlake. “The development and function of the cell plate in higher plants.” In: *Botanical Gazette* 30.3 (1900), pp. 154–170.

[19] G Yamaha. “Uber die Zytokinese bei der Pollentetradenbildung, zugleich weitere Beitrage zur Kenntnis uber die Zytokinese im Pflanzenreich”. In: *Journal of Japanese Botany* 3 (1926), pp. 139–162.

[20] Shinya Inoue. “Polarization optical studies of the mitotic spindle”. In: *Chromosoma* 5.1 (Dec. 1953), pp. 487–500. ISSN: 0009-5915.

[21] J. D. Pickett-Heaps and D. H. Northcote. “Organization of Microtubules and Endoplasmic Reticulum During Mitosis and Cytokinesis in Wheat Meristems”. In: *Journal of Cell Science* 1.1 (Mar. 1966), pp. 109–120.

[22] Chunhua Zhang, Leah E Halsey, and Daniel B Szymanski. “The development and geometry of shape change in Arabidopsis thaliana cotyledon pavement cells.” In: *BMC plant biology* 11.1 (Jan. 2011), p. 27. ISSN: 1471-2229.

[23] Chris Ambrose and Geoffrey O Wasteneys. “Nanoscale and geometric influences on the microtubule cytoskeleton in plants: thinking inside and outside the box.” In: *Protoplasma* 249 Suppl (Feb. 2012), S69–76. ISSN: 1615-6102.

[24] B Liu et al. “gamma-Tubulin in Arabidopsis: gene sequence, immunoblot, and immunofluorescence studies.” In: *The Plant cell* 6.2 (Feb. 1994), pp. 303–14. ISSN: 1040-4651.

[25] Martine Pastuglia et al. “Gamma-tubulin is essential for microtubule organization and development in Arabidopsis.” In: *The Plant cell* 18.6 (June 2006), pp. 1412–25. ISSN: 1040-4651.

[26] Natacha Janski et al. “The GCP3-interacting proteins GIP1 and GIP2 are required for γ-tubulin complex protein localization, spindle integrity, and chromosomal stability.” In: *The Plant cell* 24.3 (Mar. 2012), pp. 1171–87. ISSN: 1532-298X.

[27] M C Webb and B E Gunning. “The microtubular cytoskeleton during development of the zygote, proemhryo and free-nuclear endosperm in Arabidopsis thaliana (L.) Heynh.” In: *Planta* 184.2 (May 1991), pp. 187–95. ISSN: 0032-0935.

[28] Marisa S Otegui and L Andrew Staehelin. “Electron tomographic analysis of post-meiotic cytokinesis during pollen development in Arabidopsis thaliana.” In: *Planta* 218.4 (Feb. 2004), pp. 501–15. ISSN: 0032-0935.

[29] Jordi Chan et al. “Localization of the microtubule end binding protein EB1 reveals alternative pathways of spindle development in Arabidopsis suspension cells.” In: *The Plant cell* 17.6 (June 2005), pp. 1737–48. ISSN: 1040-4651.

[30] Yoshinobu Mineyuki, Takashi Murata, and MasamItsu Wada. “Experimental Obliteration of the Preprophase Band Alters the Site of Cell Division, Cell Plate Orientation and Phragmoplast Expansion in Adiantum Protonemata”. In: *Journal of Cell Science* 100.3 (Nov. 1991), p. 551. ISSN: 0021-9533.

[31] Jan Traas et al. “Normal differentiation patterns in plants lacking microtubular preprophase bands”. In: *Nature* 375.6533 (June 1995), pp. 676–677. ISSN: 0028-0836.

[32] Marleen Vanstraelen et al. “Cell cycle-dependent targeting of a kinesin at the plasma membrane demarcates the division site in plant cells.” In: *Current biology : CB* 16.3 (Feb. 2006), pp. 308–14. ISSN: 0960-9822.

[33] Amanda J Wright, Kimberly Gallagher, and Laurie G Smith. “discordia1 and alternative discordia1 function redundantly at the cortical division site to promote preprophase band formation and orient division planes in maize.” In: *The Plant cell* 21.1 (Jan. 2009), pp. 234–47. ISSN: 1040-4651.

[34] Lara Spinner et al. “The function of TONNEAU1 in moss reveals ancient mechanisms of division plane specification and cell elongation in land plants.” In: *Development (Cambridge, England)* 137.16 (Aug. 2010), pp. 2733–42. ISSN: 1477-9129.

[35] Juliette Azimzadeh et al. “Arabidopsis TONNEAU1 proteins are essential for preprophase band formation and interact with centrin.” In: *The Plant cell* 20.8 (Aug. 2008), pp. 2146–59. ISSN: 1040-4651.

[36] Christine Camilleri et al. “The Arabidopsis TONNEAU2 gene encodes a putative novel protein phosphatase 2A regulatory subunit essential for the control of the cortical cytoskeleton.” In: *The Plant cell* 14.4 (Apr. 2002), pp. 833–45. ISSN: 1040-4651.

[37] David Twell et al. “MOR1/GEM1 has an essential role in the plant-specific cytokinetic phragmoplast.” In: *Nature cell biology* 4.9 (Sept. 2002), pp. 711–4. ISSN: 1465-7392.

[38] J Christian Ambrose et al. “The Arabidopsis CLASP gene encodes a microtubule-associated protein involved in cell expansion and division.” In: *The Plant cell* 19.9 (Sept. 2007), pp. 2763–75. ISSN: 1040-4651.

[39] Chris Ambrose et al. “A CLASP-modulated cell edge barrier mechanism drives cell-wide cortical microtubule organization in Arabidopsis.” en. In: *Nature communications* 2 (Jan. 2011), p. 430. ISSN: 2041-1723.

[40] Stéphanie Drevensek et al. “The Arabidopsis TRM1-TON1 interaction reveals a recruitment network common to plant cortical microtubule arrays and eukaryotic centrosomes.” In: *The Plant cell* 24.1 (Jan. 2012), pp. 178–91. ISSN: 1532-298X.

[41] Pankaj Dhonukshe et al. “A PLETHORA-auxin transcription module controls cell division plane rotation through MAP65 and CLASP.” In: *Cell* 149.2 (Apr. 2012), pp. 383–96. ISSN: 1097-4172.

[42] Klementina Kakar et al. “CLASP-mediated cortical microtubule organization guides PIN polarization axis.” In: *Nature* 495.7442 (Mar. 2013), pp. 529–33. ISSN: 1476-4687.

[43] Bruce E. Shapiro et al. “Using Geometric Markers to Predict the Cell Division Plane in Meristem Cells”. In: *Proceedings of the 6th International Workshop on Functional-Structural Plant Models*. Ed. by Theodore DeJong and David Da Silva. Davis, CA, 2010, pp. 129–131.

[44] Daniel Kierzkowski et al. “Elastic domains regulate growth and organogenesis in the plant shoot apical meristem.” In: *Science* 335.6072 (Mar. 2012), pp. 1096–9. ISSN: 1095-9203.

[45] Tony J Collins. “ImageJ for microscopy”. In: *BioTechniques* 43.S1 (2007), S25–S30.

[46] SF Bockman. “Generalizing the Formula for Areas of Polygons to Moments”. In: *The American Mathematical Monthly* 96.2 (1989), pp. 131–132.

[47] L G Smith. “Plant cell division: building walls in the right places.” In: *Nature reviews. Molecular cell biology* 2.1 (Jan. 2001), pp. 33–9. ISSN: 1471-0072.

[48] Karen Alim, Olivier Hamant, and Arezki Boudaoud. “Regulatory role of cell division rules on tissue growth heterogeneity.” In: *Frontiers in plant science* 3 (Jan. 2012), p. 174. ISSN: 1664-462X.

[49] Dorota Kwiatkowska. “Structural integration at the shoot apical meristem: models, measurements, and experiments.” In: *American journal of botany* 91.9 (Sept. 2004), pp. 1277–93. ISSN: 0002-9122.

[50] L. G. Smith and S. Hake. “The Initiation and Determination of Leaves.” In: *The Plant cell* 4.9 (Sept. 1992), pp. 1017–1027. ISSN: 1532-298X.

[51] Donald E. Foard. “The initial protrusion of a leaf primordium can form without concurrent periclinal cell divisions”. In: *Canadian Journal of Botany* 49.9 (Sept. 1971), pp. 1601–1603. ISSN: 0008-4026.

[52] Colin R Goodall and Paul B Green. “Quantitative Analysis of Surface Growth”. In: *Botanical Gazette* 147.1 (1986), pp. 1–15.

[53] Viktor Blåsjö. “The Evolution of the Isoperimetric Problem”. In: *The American Mathematical Monthly* 112 (2005), pp. 526–552.

[54] Bruce E Shapiro, Elliot M Meyerowitz, and Eric Mjolsness. “Using cellzilla for plant growth simulations at the cellular level.” In: *Frontiers in plant science* 4 (Jan. 2013), pp. 1–9. ISSN: 1664-462X.

[55] Bruce E Shapiro et al. “Cellerator: extending a computer algebra system to include biochemical arrows for signal transduction simulations.” In: *Bioinformatics (Oxford, England)* 19.5 (Mar. 2003), pp. 677–8. ISSN: 1367-4803.

[56] Patrik Sahlin and Henrik Jönsson. “A modeling study on how cell division affects properties of epithelial tissues under isotropic growth.” In: *PloS one* 5.7 (Jan. 2010), e11750. ISSN: 1932-6203.

[57] Tim Rudge and Jim Haseloff. “A Computational Model of Cellular Morphogenesis in Plants”. In: *Lecture Note in Computer Science, Advances in Artificial Life*. 2005, pp. 78–87.

[58] M. E. Cunninghame and R. F. Lyndon. “The Relationship Between the Distribution of Periclinal Cell Divisions in the Shoot Apex and Leaf Initiation”. In: *Annals of Botany* 57.6 (June 1986), pp. 737–746. ISSN: 0305-7364.

[59] RF Lyndon. “Leaf formation and growth of the shoot apical meristem”. In: *Physiologie Vegetale* 10 (1972), pp. 209–222.

[60] Romain Fernandez et al. “Imaging plant growth in 4D: robust tissue reconstruction and lineaging at cell resolution.” In: *Nature Methods* May (June 2010). ISSN: 1548-7105.